Active-Region Tilt Angles: Magnetic Versus White-Light Determinations of Joy's Law

Y.-M. Wang and R. C. Colaninno

Space Science Division, Naval Research Laboratory, Washington, DC 20375, USA

yi.wang@nrl.navy.mil, robin.colaninno@nrl.navy.mil

T. Baranyi

Heliophysical Observatory, Research Centre for Astronomy and Earth Sciences, Hungarian Academy of Sciences, 4010 Debrecen, Hungary

baranyi@tigris.unideb.hu

and

J. Li

Department of Earth, Planetary, and Space Sciences, UCLA, Los Angeles, CA 90095, USA

jli@igpp.ucla.edu

ABSTRACT

The axes of solar active regions are inclined relative to the east–west direction, with the tilt angle tending to increase with latitude ("Joy's law"). Observational determinations of Joy's law have been based either on white-light images of sunspot groups or on magnetograms, where the latter have the advantage of measuring directly the physically relevant quantity (the photospheric field), but the disadvantage of having been recorded routinely only since the mid-1960s. White-light studies employing the historical Mount Wilson (MW) database have yielded tilt angles that are smaller and that increase less steeply with latitude than those obtained from magnetic data. We confirm this effect by comparing sunspot-group tilt angles from the Debrecen Photoheliographic Database with measurements made by Li and Ulrich using MW magnetograms taken during cycles 21–23. Whether white-light or magnetic data are employed, the median tilt angles significantly exceed the mean values, and provide a better characterization of the observed distributions. The discrepancy between the white-light and magnetic results is found to have two main sources. First, a substantial

fraction of the white-light "tilt angles" refer to sunspots of the same polarity. Of greater physical significance is that the magnetograph measurements include the contribution of plage areas, which are invisible in white-light images but tend to have greater axial inclinations than the adjacent sunspots. Given the large uncertainties inherent in both the white-light and the magnetic measurements, it remains unclear whether any systematic relationship exists between tilt angle and cycle amplitude during cycles 16–23.

Subject headings: Sun: activity — Sun: faculae, plages — Sun: magnetic fields — Sun: photosphere — sunspots

1. INTRODUCTION

As toroidal magnetic flux rises buoyantly through the convection zone to form sunspots and active regions, the Coriolis force acts to twist the flux tubes so that they emerge slightly inclined relative to the east–west direction (see, e.g., Caligari et al. 1995; D'Silva & Choudhuri 1993; Fan et al. 1994; Fisher et al. 1995; Wang & Sheeley 1991). This axial tilt plays a central part in flux-transport dynamo models, where it is an essential ingredient in the formation and evolution of the polar fields (see, e.g., Wang & Sheeley 1991; Dikpati & Charbonneau 1999; Mackay et al. 2002; Baumann et al. 2004; Cameron et al. 2010; Muñoz-Jaramillo et al. 2010, 2013; Jiang et al. 2011a, 2011b, 2013, 2014; Kitchatinov & Olemskoy 2011; Cameron & Schüssler 2012; Hathaway & Upton 2014; Upton & Hathaway 2014a, 2014b).

The tendency for the leading/westward parts of sunspot groups to be located equatorward of their trailing/eastward parts was first studied by Joy, using the sunspot drawings of Carrington and Spörer made between 1856 and 1893 (cycles 10–13). From the data listed in Table II of Hale et al. (1919), we infer that the 2633 sunspot groups measured by Joy had an area-weighted average inclination of $6\overset{\circ}{.}1$; a linear fit to the tilt angles as a function of latitude L gives

$$\gamma(L) = 0.27|L| + 1\overset{\circ}{.}9 \tag{1}$$

over the range $0 < |L| < 30^\circ$. By definition,

$$\tan\gamma = \frac{\Delta L}{\Delta\phi \cos L}, \tag{2}$$

where ΔL is the latitudinal separation between the leading and trailing poles of the sunspot group or active region, $\Delta\phi$ is their longitudinal separation, and γ is taken to be positive

if the leading pole lies equatorward of the trailing pole (in either hemisphere), negative otherwise. This definition restricts the tilt angles to the range $-90^\circ \leq \gamma \leq +90^\circ$, and does not distinguish between different polarity orientations, so that it is suited for white-light measurements in which the polarities are unknown. Hale et al. (1919) noted that "the angle of inclination was found to depend entirely on the latitude of the group, without reference to the number of the cycle or the time within the cycle. A knowledge of the polarities of the spots would have aided greatly in determining the position of the axes of the groups."

Joy's results, as reported in Hale et al. (1919), were subsequently confirmed by Brunner (1930), using drawings of 1981 sunspot groups made at the Zürich Observatory between 1894 and 1928 (cycles 13–16). Brunner obtained a value of $\gamma_{\rm mean} = 6\overset{\circ}{.}5$ for the mean tilt angle of his entire sample; a linear fit to the latitudinally binned data in his Table I yields

$$\gamma(L) = 0.51|L| - 0\overset{\circ}{.}8, \tag{3}$$

the slope thus being considerably steeper than that found by Joy. It should be noted that the derived slopes depend sensitively on the relatively few measurements made at very low and very high latitudes: thus, for the 0°–5° (25°–30°) latitude bin, Brunner obtained a mean tilt angle of $0\overset{\circ}{.}6$ ($14\overset{\circ}{.}4$), whereas Joy's measurements gave $3\overset{\circ}{.}7$ ($9\overset{\circ}{.}3$), leading to a much flatter slope. According to Brunner, the average axial tilts of sunspot groups decrease systematically from $\sim 7\overset{\circ}{.}8$ to $\sim 4\overset{\circ}{.}6$, as they evolve from small spots/pores without penumbrae to large, widely separated spots. In contrast, Hale et al. (1919) stated that "there is little change in this angle during the life of the group."

Joy's law was confirmed using magnetograph measurements by Wang & Sheeley (1989, 1991), who analyzed the statistical properties of 2710 bipolar magnetic regions (BMRs) that appeared in daily full-disk magnetograms recorded by the National Solar Observatory at Kitt Peak (NSO/KP) during cycle 21 (1976–1986). Here, the centroidal positions of the positive- and negative-polarity flux were estimated visually by Sheeley from photographic prints, with the help of Stonyhurst overlay grids. The BMR tilt angles were found to increase with latitude with a slope of approximately 0.5, close to the value obtained by Brunner (1930); averaged over the entire data set, $\gamma_{\rm mean}$ was as large as 9°. An important difference from most other tilt-angle studies is that each BMR was measured only once, at or as close as possible to the time when its flux reached its peak (the original purpose having been to provide a source term for surface flux-transport modeling). By tracking the day-to-day evolution of the flux by eye, it was usually possible to distinguish between closely spaced active regions, which is often not the case when automated methods are employed.

Howard (1989, 1991a) applied a field-strength thresholding algorithm to identify active regions in coarse-format versions of Mount Wilson (MW) Observatory daily magnetograms recorded during 1967–1990, and then derived their axial tilts from the flux-weighted positions

of their leading and trailing sectors. He obtained a less regular increase in the tilt angle with latitude than Wang & Sheeley (1989), and suggested that the difference might be due to the inclusion of older, decayed regions in his sample.

From an analysis of 517 BMRs appearing on magnetograms taken at the Huairou Solar Observing Station during 1988–2001, Tian et al. (2003) derived a Joy's law slope of 0.5, in good agreement with the results of Wang & Sheeley (1989, 1991). The active regions in this study were selected for measurement when they were "almost mature" and located within 15° of central meridian.

More recently, Stenflo & Kosovichev (2012) and Li & Ulrich (2012) developed automated procedures to derive active-region tilt angles from magnetograms recorded with the Michelson Doppler Imager (MDI) on the *Solar and Heliospheric Observatory* (*SOHO*), finding slopes of ∼0.56 and 0.36, respectively, for Joy's law. Li & Ulrich (2012) also applied their algorithm to MW magnetograms taken during 1974–2012, obtaining a slope of 0.45 and a mean tilt angle of 6.°2.

Howard (1991b) derived tilt angles for sunspot groups appearing in MW daily white-light photographs taken between 1917 and 1985.[1] Here, the umbral positions and areas were measured and grouped by proximity as described in Howard et al. (1984); the umbrae located westward (eastward) of the area-weighted centroid of each group were then defined as belonging to the "leading" ("following") sector (despite the absence of polarity information). As may be seen from Figure 3 in Howard (1991b), the white-light tilt angles show a fairly regular increase up to latitude $|L| \sim 30°$, but the average slope is only about one-half that shown in Figure 5 of Howard (1991a) for the tilts derived from MW magnetograms. Reviewing his white-light and magnetic results, Howard (1996) noted that the average tilt angle based on the 24,308 MW sunspot-group measurements over the period 1917–1985 was $\gamma_{\rm mean} = 4.°3$, whereas the corresponding value for the 15,692 "plages" in MW magnetograms taken during 1967–1995 was $\gamma_{\rm mean} = 6.°3$.

Employing the MW sunspot-group tilt-angle measurements and the analogous Kodaikanal (KK) database covering the period 1906–1987, Dasi-Espuig et al. (2010) derived a slope of 0.26/0.28 (MW/KK) for Joy's law and a mean tilt angle of 4.°25/4.°5 (MW/KK). In addition, they found a tendency for $\gamma_{\rm mean}/|L|_{\rm mean}$, the mean tilt angle normalized by the mean latitude of the sunspot groups, calculated for each of cycles 15–21, to decrease with increasing cycle strength. From the Pulkovo database of sunspot group measurements during 1948–1991, Ivanov (2012) obtained a Joy's law slope of 0.38 and a mean tilt angle of 6.°1. He also showed that the anticorrelation between $\gamma_{\rm mean}/|L|_{\rm mean}$ and cycle strength in

[1]See `ftp://ftp.ngdc.noaa.gov/STP/SOLAR_DATA/ SUNSPOT_REGIONS/Mt_Wilson_Tilt`.

the MW data is almost entirely due to the unusually low value of $\gamma_{\rm mean}$ during cycle 19 (see also the corrigendum of Dasi-Espuig et al. 2013; a strong anticorrelation remains present in the normalized KK tilt angles for cycles 15–21). In their study of hemispheric asymmetries in the MW sunspot-group tilt angles, McClintock & Norton (2013) found that the mean value of γ during cycle 19 was $4\overset{\circ}{.}6$ in the northern hemisphere, but only $1\overset{\circ}{.}8$ in the southern hemisphere. In line with the results of Dasi-Espuig et al. (2010) and the flux transport simulations of Schüssler & Baumann (2006), they also advocated a downward revision in the slope of Joy's law.

From this brief review, we infer that the active-region tilt angles derived from magnetograms have tended to be systematically larger than those deduced from white-light observations. As an apparent exception, the sunspot group measurements of Brunner (1930) are in accord with the magnetograph results. However, an inspection of Brunner's Table III suggests that roughly one-third of his measurements were made at a very early, pre-penumbral stage in the evolution of the sunspot groups, when their mean tilt was as large as $7\overset{\circ}{.}8$. Such emerging regions, which consist of small, faint sunspot pores, are likely to constitute a much smaller fraction of the sunspot groups in the MW and KK databases, which are presumably dominated by fully developed regions whose tilt angles have an average value of $4\overset{\circ}{.}6$, according to Table III of Brunner (1930). Since the statistical studies of magnetic tilt angles are also heavily weighted toward fully emerged active regions, the good agreement between Brunner's results and those of Wang & Sheeley (1989, 1991), Tian et al. (2003), Li & Ulrich (2012), and Stenflo & Kosovichev (2012) could be partly fortuitous.

The main objective of this study is to understand why white-light observations of sunspot groups tend to yield smaller tilt angles than magnetograph measurements of active regions. For this purpose, we compare the tilt angles given in the Debrecen Photoheliographic Data (DPD) sunspot catalog[2] with the corresponding values derived by Li & Ulrich (2012) from MW magnetograms taken during cycles 21–23 (Section 2). Section 3 places these recent magnetic and white-light tilt-angle measurements in the context of the MW white-light results for cycles 16–21. In Section 4, we examine specific cases in which the white-light and magnetic measurements give very different tilt angles, and discuss how such systematic differences arise. Our results are summarized in Section 5.

[2]See `http://fenyi.solarobs.unideb.hu/DPD`. The DPD database represents a continuation of the Greenwich Photoheliographic Results (1874–1976).

2. COMPARISON OF WHITE-LIGHT AND MAGNETIC TILT ANGLES DURING CYCLES 21–23

The online DPD catalog contains daily measurements of sunspot areas and positions from 1974 to the present, based on full-disk white-light images taken mainly at the Debrecen Observatory and its Gyula Observing Station (see Győri et al. 2011). The database also provides sunspot-group tilt angles derived in two different ways: (1) from the area-weighted umbral positions alone ("U"), as in the case of the MW and KK sunspot-group tilt angles; and (2) from the area-weighted positions of all visible components of the sunspot group, including umbrae, penumbrae, and pores ("UPP").[3] Again, the "leading" and "following/trailing" portions of a sunspot group are defined relative to the area-weighted centroid of the group, and do not necessarily coincide with the actual leading- and trailing-polarity sectors of the active region. We also remark that the number of DPD/UPP tilt-angle measurements considerably exceeds (by ∼70%) the number of DPD/U measurements, because many sunspot groups contain at least a few faint pores, but only one umbra (usually in the leading sector) or, in a roughly equal number of cases, no umbrae at all.

In addition to DPD, the Debrecen Observatory team has constructed a database that employs MDI continuum images and magnetograms recorded during 1996–2011. The *SOHO*/MDI Debrecen Data (SDD) sunspot catalog provides four kinds of tilt angle measurements, two of which use only the continuum intensity images and are exactly analogous to DPD/U and DPD/UPP. The remaining two types of tilt angle estimates exploit the MDI magnetograms to assign polarities to the U and UPP continuum measurements, so that the leading and following sectors are distinguished by polarity instead of being defined by the area-weighted centroid of the sunspot group. Because the statistical properties of the SDD and DPD tilt angles turn out to be rather similar, however, this study will focus on the DPD database, which covers three complete sunspot cycles. A detailed analysis of the SDD and DPD measurements and comparison with MW/KK may be found in Baranyi (2014).

Employing daily full-disk MW magnetograms recorded between 1974 and 2012, Li & Ulrich (2012) determined the tilt angles of active regions based on the flux-weighted centroids of the leading- and trailing-polarity sectors. Since the period that they studied nearly coincides with that covered by the DPD database, it is interesting to compare their magnetic tilt angles ("MW/MAG") with the DPD white-light results.

Let the tilt angles derived from the DPD/U, DPD/UPP, and MW/MAG measurements

[3]The DPD catalog designates the combination of umbral and non-umbral areas by "whole spot" or "WS" (formerly "U+P"). However, to emphasize that the non-umbral areas include small pores as well as penumbrae, we here employ the acronym "UPP" (umbrae, penumbrae, and pores) instead of "WS."

be designated by $\gamma_{\rm U}$, $\gamma_{\rm UPP}$, and $\gamma_{\rm mag}$, respectively. Throughout this study, we include only measurements made within 45° of longitude from central meridian, so as to avoid distortions due to foreshortening near the solar limb. To determine the latitudinal dependence of the tilt angles, we bin the measurements into 5°-wide intervals of unsigned latitude $|L|$, and calculate either the arithmetic mean or the median of the data within each bin. When performing averages, we follow the convention of treating multiple measurements of a single active region as if they represented measurements of different active regions (instead of combining them into one value), even though this procedure gives greater weight to longer-lived regions.

We begin by examining the average behavior of the tilt angles over the entire interval from 1976 June through 2008 December, comprising cycles 21–23. For this 32 yr period, Li & Ulrich (2012) made a total of 25,322 measurements of $\gamma_{\rm mag}$ based on 7958 active regions; the DPD database provides 23,204 measurements of $\gamma_{\rm U}$ for 5973 NOAA sunspot groups, and 38,975 measurements of $\gamma_{\rm UPP}$ for 8575 NOAA sunspot groups. (Although the DPD catalog also contains sunspot groups without NOAA designations, we omit them in order to maximize the overlap with the active region sample of Li and Ulrich.) Figure 1 shows $\gamma_{\rm mag}$, $\gamma_{\rm U}$, and $\gamma_{\rm UPP}$ as a function of $|L|$. In the top panel, arithmetic means of the tilt angles are plotted for each latitude bin between 0°–5° and 30°–35°, while median values are plotted in the bottom panel. The standard error of the mean/median is indicated by the vertical bar through each point; the errors are largest for the highest- and lowest-latitude bins because they contain the smallest number of measurements. The straight lines represent least-squares fits to the plotted points up to latitude $|L| = 30°$; the point at 30°–35° is omitted both because it is based on relatively few measurements, and because it may be significantly affected by differential rotation, which acts to decrease the tilt angles with time and has its steepest gradients at midlatitudes. The slope $m_{\rm Joy}$ and y-intercept b_0 of the regression line then define Joy's law for the given set of tilt angle measurements:

$$\gamma(L) = m_{\rm Joy}|L| + b_0. \tag{4}$$

From Figure 1, the magnetic tilt angles ($\gamma_{\rm mag}$) are seen to increase more steeply than those derived from white-light observations ($\gamma_{\rm U}$, $\gamma_{\rm UPP}$). In addition, regardless of whether magnetic or white-light data are used, the median values yield systematically larger slopes $m_{\rm Joy}$ than the mean values.

If the tilt angle measurements for all latitudes are now combined, we find that the mean values of $\gamma_{\rm mag}$, $\gamma_{\rm U}$, and $\gamma_{\rm UPP}$ during cycles 21–23 are $6\overset{\circ}{.}2 \pm 0\overset{\circ}{.}2$, $5\overset{\circ}{.}3 \pm 0\overset{\circ}{.}2$, and $5\overset{\circ}{.}9 \pm 0\overset{\circ}{.}1$, respectively, while their median values are $7\overset{\circ}{.}5 \pm 0\overset{\circ}{.}2$, $6\overset{\circ}{.}6 \pm 0\overset{\circ}{.}2$, and $6\overset{\circ}{.}9 \pm 0\overset{\circ}{.}2$ (all quoted errors are 1σ). Thus the magnetic tilt angles are systematically larger than their white-light counterparts, and the median values are systematically larger than the mean values for both

magnetic and white-light tilts. The white-light tilt angles derived from umbral, penumbral, and pore positions are slightly larger than those derived from umbral positions only.

Both magnetic and white-light tilt angles exhibit an extremely wide scatter, due both to measurement errors and to the randomizing effect of the ambient supergranular convection; in general, the root-mean-square (rms) tilt angles are much larger than their arithmetic means, and increase with decreasing BMR size or total flux (see Howard 1989, 1991a, 1991b, 1996; Wang & Sheeley 1989, 1991). Figure 2 shows histograms of $\gamma_{\rm mag}$, $\gamma_{\rm U}$, and $\gamma_{\rm UPP}$, again including all measurements taken during cycles 21–23. The bin width is 5°, and each histogram (plotted as a smooth curve connecting the discrete bin values) has been normalized by dividing by the total number of measurements and multiplying by a constant scaling factor. All three tilt-angle distributions exhibit a Gaussian-like profile, with peak located in the 5°–10° bin and a half width at half-maximum (HWHM) ranging from 15.°4 (DPD/U) to 17.°5 (MW/MAG). (Despite their Gaussian appearance, however, the distributions are not well fitted by single Gaussian functions.) Because the peak is shifted to the right of $\gamma = 0$, the wings of the profile are not symmetric over the range $-90° < \gamma < +90°$, and the "outliers" near the left/negative end of the distribution act to decrease the mean value of γ relative to the median value. To represent the centroid of such skewed distributions, it is preferable to employ the median (as was done by Li & Ulrich 2012) rather than the mean. From a physical viewpoint, we note that a nonnegligible fraction of the negative outliers are likely to represent BMRs with reversed ("anti-Hale") east–west polarity orientations, which would be assigned tilt angles $\gamma > +90°$ if a polarity-dependent definition were adopted, in which γ ranges between $-180°$ and $+180°$. In the absence of the artificial cutoff at $\pm 90°$, the mean of the distribution would then increase and converge toward the median. It should be remarked that the great majority of extreme outliers beyond $|\gamma| \sim 60°$ are associated with small active regions having leading–following separations of less than 2.°5.

Although the distributions of $\gamma_{\rm mag}$, $\gamma_{\rm U}$, and $\gamma_{\rm UPP}$ have remarkably similar, quasi-Gaussian profiles, the curves of Figure 2 deviate significantly from each other around their peaks and for relatively large, positive tilt angles. In particular, MW/MAG shows a "deficit" of tilt angles in the range ∼0°–15° but a "surplus" in the range ∼25°–40°, as compared to DPD/UPP and especially DPD/U. From the fact that tilt angles of ∼25°–40° are characteristic of active regions located at mid to high latitudes, we infer that such active regions (typically associated with the rising phase of the cycle) may be an important source of the differences among the three distributions, as is also suggested by Figure 1.

We now consider the behavior of the tilt angles for the individual cycles. In the top panel of Figure 3, we plot the median values of $\gamma_{\rm mag}$ as a function of $|L|$ separately for cycles 21, 22, and 23; the middle and bottom panels display the corresponding results for $\gamma_{\rm U}$

and $\gamma_{\rm UPP}$, respectively. Neither the magnetic nor the white-light tilt angles show any clear evidence for systematic variations among these three cycles (which, it should be remarked, have rather similar sunspot-number amplitudes). In the case of the tilt angles derived from MW magnetograms, the slope $m_{\rm Joy}^{\rm (med)}$ ranges from 0.47 ± 0.05 (cycle 22) to 0.57 ± 0.03 (cycle 21); the median tilt angle based on all latitudes, $\gamma_{\rm med}$, ranges from $7\overset{\circ}{.}1 \pm 0\overset{\circ}{.}3$ (cycle 23) to $7\overset{\circ}{.}8 \pm 0\overset{\circ}{.}4$ (cycle 22). In the case of the tilt angles derived from umbral data alone, $m_{\rm Joy}^{\rm (med)}$ varies from 0.34 ± 0.02 (cycle 21) to 0.46 ± 0.06 (cycle 22), while $\gamma_{\rm med}$ varies from $6\overset{\circ}{.}0 \pm 0\overset{\circ}{.}4$ (cycle 22) to $7\overset{\circ}{.}0 \pm 0\overset{\circ}{.}4$ (cycle 23). When penumbral areas and pores are included, $m_{\rm Joy}^{\rm (med)}$ varies from 0.36 ± 0.03 (cycle 21) to 0.44 ± 0.04 (cycle 23), and $\gamma_{\rm med}$ varies from $6\overset{\circ}{.}5 \pm 0\overset{\circ}{.}3$ (cycle 22) to $7\overset{\circ}{.}4 \pm 0\overset{\circ}{.}3$ (cycle 23). Thus $m_{\rm Joy}^{\rm (med)}$ has its largest value in cycle 21 according to the magnetic measurements, in cycle 22 when umbral positions alone are used, but in cycle 23 when umbral, penumbral, and pore data are employed; on the other hand, $\gamma_{\rm med}$ has its largest value in cycle 22 according to the magnetic observations, but in cycle 23 according to both sets of white-light observations. These seemingly random differences give some indication of the uncertainties involved in attempting to deduce systematic long-term trends from tilt angle measurements.

The tilt angle statistics described here and in the next section are summarized in Tables 1 and 2.

3. COMPARISON WITH THE MW SUNSPOT-GROUP DATABASE

The tilt angles derived from the sunspot-group measurements of Howard et al. (1984), using daily white-light photographs taken at MW during 1917–1985, have been analyzed previously by Howard (1991b, 1996), Dasi-Espuig et al. (2010), Ivanov (2012), and McClintock & Norton (2013). Because Howard et al. (1984) measured the positions and areas of umbrae only, this data set, referred to here as "MW/WL," may be considered analogous to DPD/U. It is clearly of interest to compare the MW/WL tilt angles with those derived from the more recent databases. For this purpose, we divide the MW/WL time series into six cycles, starting with cycle 16 (1923 August–1933 August) and ending with cycle 21 (1976 June–1986 August); we discard the observations for cycle 15, since they do not include its rising phase, and we assume that the data gap during the final months of cycle 21 does not significantly affect the overall statistics for that cycle. We omit all measurements taken more than 45° from central meridian longitude, as well as those for which the centroids of the leading and following parts are separated by an angle $\Delta s = [(\Delta\phi \cos L)^2 + (\Delta L)^2]^{1/2}$ exceeding 20°, which is the maximum pole separation among the BMRs analyzed by Wang & Sheeley (1989; see their Figure 2, and also the discussion of Dasi-Espuig et al. 2010).

To derive Joy's law for each cycle, we again compute the mean or median value of γ within 5°-wide bins in $|L|$ and apply a linear least-squares fit over the latitude range 0°–30°.

Figure 4 (top panel) shows the Joy's law slope, $m_{\rm Joy}$, derived for each of cycles 16–21 by fitting the mean values of γ as a function of $|L|$. Also plotted for comparison are the corresponding slopes obtained for cycles 21–23 from the DPD/U, DPD/UPP, and MW/MAG measurements. As a reminder of the relative strengths of the different cycles, the asterisks indicate the (arbitrarily scaled) maximum yearly sunspot number $R_{\rm max}$ for each cycle. The bottom panel of Figure 4 displays the same quantities, but with $m_{\rm Joy}$ determined from the median rather than the mean value of the tilt angle as a function of latitude.

From Figure 4, we see that the Joy's law slopes obtained from the MW/WL sunspot-group data tend to be substantially smaller than those determined from both the DPD and the magnetic measurements. Averaged over cycles 16–21, the mean-based (median-based) MW/WL slope is $m_{\rm Joy} = 0.20 \pm 0.01$ (0.27 ± 0.01),[4] whereas the corresponding value for DPD/U, averaged over cycles 21–23, is $m_{\rm Joy} = 0.28 \pm 0.03$ (0.40 ± 0.04). However, for cycle 21, the only period when the databases overlap, MW/WL actually gives a larger slope than DPD/U; the significance of this "convergence" is unclear to us.

Figure 5 (top panel) displays the mean values of γ, averaged over each cycle and over all latitudes, for the different data sets; the median values are plotted in the bottom panel. When averaged over cycles 16–21, the MW/WL tilt angles have a mean (median) value of $4\overset{\circ}{.}4 \pm 0\overset{\circ}{.}2$ ($5\overset{\circ}{.}8 \pm 0\overset{\circ}{.}2$), roughly 1° smaller than the corresponding DPD values averaged over cycles 21–23, and ∼2° smaller than the MW/MAG values. Again, the different data sets are in relatively good agreement for cycle 21, when the MW/WL tilt angles attain their highest cycle-averaged values. We note that the DPD tilt angles for cycle 21 remain almost unchanged even if the 1986 measurements are omitted when averaging over this cycle; thus it is unlikely that the agreement can be attributed to the absence of MW/WL data in 1986.

As pointed out by Dasi-Espuig et al. (2010), the cycle-averaged values of γ depend on the latitudinal distribution of the measured active regions, which may vary from cycle to cycle and from one database to another. To correct for this effect (following Dasi-Espuig et al.), we now divide the cycle-averaged tilt angles by their corresponding cycle-averaged, unsigned latitudes. Figure 6 shows the resulting normalized quantities, $\gamma_{\rm mean}/|L|_{\rm mean}$ (top panel) and $\gamma_{\rm med}/|L|_{\rm med}$ (bottom panel). The latitude normalization considerably reduces the cycle-to-cycle variations and the differences between the various data sets. This partial

[4]The value of $m_{\rm Joy}^{\rm (mean)}$ derived by Dasi-Espuig et al. (2010) from the MW/WL data (0.26) is higher than ours (0.20) because they forced their least-squares fit to pass through zero, setting $b_0 = 0$ in Equation (4) (see also the discussion of McClintock & Norton 2013).

convergence reflects the fact that, averaged over cycles 16–21, the MW/WL measurements were made at a mean (median) latitude of 15.°1 (14.°4), as compared to 15.°9 (15.°3) for the DPD measurements, averaged over cycles 21–23.

Even after the latitude normalization is applied, it is clear from Figure 6 that cycle 19 remains an outlier characterized by unusually small values of $\gamma_{\rm mean}/|L|_{\rm mean}$ and $\gamma_{\rm med}/|L|_{\rm med}$, according to the MW/WL measurements. For comparison, as indicated by Figure 4(c) in Ivanov (2012), the Pulkovo measurements for this cycle give $\gamma_{\rm mean}/|L|_{\rm mean} \simeq 0.40$, twice the MW/WL value. However, it should also be noted that the Pulkovo data coverage of cycle 19 is incomplete, with Figure 3 of Ivanov (2012) showing a gap that extends through the maximum phase 1957–1960. As pointed out by McClintock & Norton (2013), the unusually low MW/WL value for cycle 19 is mainly attributable to the southern-hemisphere sunspot groups, which have a latitude-normalized mean tilt angle of 0.15, as compared to 0.26 for the northern hemisphere. In flux transport models, the evolution of the polar fields depends sensitively on the tilt angles of active regions and on the meridional flow speed. The magnetograph observations of Babcock (1959) indicate that the south polar field reversed as early as mid-1957, whereas the north polar field reversed in late 1958 (see also the polar faculae counts of Sheeley 2008). This timing seems difficult to reconcile with the very small tilt angles that the MW/WL database assigns to the southern hemisphere, unless large variations in the meridional flow speed are invoked.

In Figure 7, we have plotted a histogram of the 22,533 MW/WL tilt-angle measurements made during cycles 16–21; for comparison, we again display the histogram of the 23,204 DPD/U tilt angles measured during cycles 21–23. The MW/WL tilt angles show a significantly larger scatter, with the Gaussian-like distribution having a HWHM of 17.°9, as compared to 15.°4 for the DPD/U measurements.

From a sample of MW white-light images and sunspot-group drawings with polarity labeling[5] for the period 1961–1967, Baranyi (2014) found that ∼84% of the sunspot groups whose leading and following parts had separations $\Delta s < 2.°5$ consisted entirely of spots of the same polarity. In the great majority of these "unipolar" groups, the actual opposite-polarity (usually trailing) sector contained no visible umbrae; in the remaining cases, the two sectors of a larger sunspot group were incorrectly taken to be separate groups. Based on all of the MW/WL measurements made within 45° of central meridian during cycles 16–21, the median angular separation of the leading and following sectors is only 2.°9, and 43% of

[5]See `ftp://howard.astro.ucla.edu/pub/obs/drawings`. The extensive information contained in these drawings, which identify each sunspot group and indicate the positions, areas, polarities, and strengths of most of the individual sunspots/pores recorded since 1917, has recently been tabulated by Tlatov et al. (2014).

the sunspot groups have $\Delta s < 2.^\circ5$. As may be seen from the red dotted curve in Figure 8, the tilt angle distribution of these "compact" groups is extremely broad (HWHM = $25.^\circ7$); furthermore, the mean (median) value of γ is only $2.^\circ7$ ($4.^\circ0$), as compared to $4.^\circ4$ ($5.^\circ8$) for all sunspot groups. When this component is separated out and only sunspot groups having $\Delta s > 2.^\circ5$ are retained, the HWHM of the original tilt-angle distribution decreases from $17.^\circ9$ to $16.^\circ6$, and the outliers in the far wings $|\gamma| \gtrsim 60^\circ$ almost disappear (compare the black solid and blue dashed curves in Figure 8).

After filtering out sunspot groups with $\Delta s < 2.^\circ5$ from the MW/WL database, we find that $\gamma_{\rm mean}$ ($\gamma_{\rm med}$) increases from $4.^\circ4$ ($5.^\circ8$) to $5.^\circ8$ ($6.^\circ4$), while $\gamma_{\rm mean}/|L|_{\rm mean}$ ($\gamma_{\rm med}/|L|_{\rm med}$) increases from 0.29 (0.40) to 0.38 (0.45); likewise, $m_{\rm Joy}^{\rm (mean)}$ ($m_{\rm Joy}^{\rm (med)}$) increases from 0.20 (0.27) to 0.32 (0.34). When the same procedure is applied to the DPD/U measurements for cycles 21–23, for which 33% of the sunspot groups have $\Delta s < 2.^\circ5$, $\gamma_{\rm mean}$ ($\gamma_{\rm med}$) increases from $5.^\circ3$ ($6.^\circ6$) to $6.^\circ4$ ($7.^\circ0$), $\gamma_{\rm mean}/|L|_{\rm mean}$ ($\gamma_{\rm med}/|L|_{\rm med}$) increases from 0.33 (0.43) to 0.40 (0.45), and $m_{\rm Joy}^{\rm (mean)}$ ($m_{\rm Joy}^{\rm (med)}$) increases from 0.28 (0.40) to 0.40 (0.45). The filtering has a smaller effect on the tilt angles derived from the DPD/UPP measurements, for which only 23% of the sunspot groups have $\Delta s < 2.^\circ5$. In all cases, the median tilt angles undergo considerably less change than the corresponding means, again suggesting that the median provides a more robust statistical measure than the mean. Figure 9 shows the overall effect of omitting sunspot groups with $\Delta s < 2.^\circ5$ on the Joy's law slopes derived from the different databases (compare Figure 4). We note that only 11% of the MW/MAG measurements have the leading- and trailing-polarity centroids separated by less than $2.^\circ5$, consistent with the conclusion of Baranyi (2014) that most of the MW/WL measurements having $\Delta s < 2.^\circ5$ refer to "unipolar" sunspot groups.

Although filtering out the unipolar groups brings the different data sets into better agreement with each other, the magnetic measurements still appear to provide an upper bound on the tilt angles (see Tables 1 and 2). The physical basis of the remaining discrepancy is discussed in Section 4.

4. CONTRIBUTION OF PLAGE AREAS TO MAGNETIC TILT ANGLES

Even when new active regions are at their peak development, only ∼50% of their magnetic flux is contained in sunspots (Schrijver 1987; Sheeley 1966), with the rest being in the form of plages/faculae, which are invisible in white-light images except near the solar limb. Plages, best seen in Ca II K-line spectroheliograms, represent very strong fields that fall below the ∼1500 G threshold for sunspots. We now consider the possibility that the magnetic tilt angles tend to be larger than their white-light counterparts because the magnetograph

measurements include the contribution of plage areas. For this purpose, we examine a number of specific cases in which magnetic and white-light measurements have been carried out for the same active region, but with very different results. These examples are all taken from the rising phase of the activity cycle, when the tilt angles and the discrepancies between the measurements tend to be greatest.

Figure 10 shows a white-light image of active region NOAA 807, as recorded by the Debrecen Observatory on 1977 April 18; also displayed are longitudinal magnetograms from MW (spatial resolution 3.″7/pixel) and NSO/KP (∼1″/pixel) taken on the same day. The region is centered at latitude $L \simeq -20°$, and is dominated by a pair of leading sunspots separated by 4.°5. For this sunspot group, the tilt angles given by the DPD/U and DPD/UPP databases are 2.°5 and 1.°8, respectively; in contrast, Li & Ulrich (2012) obtained a value of γ as large as 30° from the MW magnetogram, in agreement with the measurement by Sheeley from the KP magnetogram (see Wang & Sheeley 1989). To show why the white-light and magnetic results are so different, we have overplotted on each of the images in Figure 10 the axes connecting the centroids of the leading and following sectors, according to DPD/U, Li & Ulrich (MW/MAG), and Sheeley (KP/MAG). It is evident that the white-light tilt angles are so small because the easternmost of the two sunspots is incorrectly assigned to the following sector. From the magnetograms, we see that both spots have leading (negative) polarity, while the trailing-polarity sector, centered to the southeast of the sunspot pair, consists mainly of plage and is almost invisible in the white-light image.

Figure 11 displays a Debrecen white-light image of active region NOAA 882, together with the corresponding MW and KP magnetograms. The region is centered at $L \simeq +24°$, and the observations were all made on 1977 September 5. A prominent sunspot is seen only in the leading sector. The tilt angles measured by DPD/U, DPD/UPP, MW/MAG, and KP/MAG are 12°, 19°, 29°, and 39°, respectively. The DPD/U tilt-angle measurement (not shown) can be rejected because it takes the following sector to be centered on a small satellite umbra within the leading sunspot, so that $\Delta s \sim 0.°3$. The DPD/UPP measurement takes into account the small pores in the trailing-polarity sector, but not the extensive plage areas; the inferred axis (red line in Figure 11) is thus less steeply inclined than the axes derived from the MW and KP magnetograms (indicated by the blue and green lines, respectively).

Figure 12 shows a Debrecen image of NOAA 1203 on 1978 July 14, along with the corresponding MW and KP magnetograms. For this active region, centered at $L \simeq +18°$, the tilt angles given by DPD/U, DPD/UPP (not shown), MW/MAG, and KP/MAG are 6°, 5°, 21°, and 19°, respectively. Here, it is again clear that the axial inclination of the BMR cannot be deduced from the white-light image in the absence of polarity information. In this case, the large structure dominating the eastern part of the sunspot group encloses spots of

both polarities, so that the basic assumption underlying the white-light measurements—that sunspots of opposite polarity do not overlap in longitude—breaks down. The DPD tilt angles are too small because all of the spots located eastward of the area-weighted centroid of the sunspot group have automatically been assigned to the following-polarity sector.

As an example from the rising phase of cycle 23, Figure 13 shows a continuum image and magnetogram of active region NOAA 8086, located at $L \simeq +28°$. Both images were recorded by *SOHO*/MDI on 1997 September 17. The sunspot group again consists of a prominent leading spot trailed by a smattering of smaller spots/pores. The DPD and SDD measurements all give values of γ in the range $\sim$19°–23°; the SDD/U tilt angle is indicated by the red line connecting the leading spot to the pores located to its northeast. In contrast, based on the MDI magnetogram, Li & Ulrich (2012) derived a tilt angle of 41° (indicated by the blue line). This steeper inclination reflects the presence of (positive) leading-polarity plage to the east of the large leading spot and (negative) trailing-polarity plage to the west of the small trailing spots.

From these case studies, it is clear that the use of white-light observations to derive tilt angles is subject to many pitfalls, and that the results often do not reflect the actual axial inclinations of active regions, as defined by the distribution of magnetic field. One of the main sources of error is the well-known asymmetry between the leading- and following-polarity sectors, with the latter being characterized by smaller spots and less concentrated flux (more extensive plage areas) (see Fan et al. 1993, and references therein; Muraközy et al. 2014). If only the darkest features (umbrae) are used to determine the centroids of the two sectors, as is the case for the MW/WL and DPD/U data sets, spots belonging to the leading-polarity sector may be assigned to the following sector, particularly when there are no visible umbrae of following polarity (as in Figure 10). Moreover, the absence of tilt angle measurements when only a single (or no) umbra is observed reduces the size of the sample by as much as $\sim$40%, introducing an unknown bias into the statistics. Another major source of error is associated with active regions where sunspots of opposite polarity overlap in longitude, as in Figure 12. In such cases, in the absence of polarity information, the white-light measurements will tend to underestimate the actual tilt angles.

As illustrated by the examples of Figures 10, 11, and 13, a more fundamental shortcoming of the white-light measurements is that they do not include the contribution of plage areas. That the plage component of active regions tends to have a greater axial inclination than the sunspot component was pointed out earlier by Howard (1996), who compared a histogram of tilt angles derived from MW magnetograms taken during 1967–1995 with the tilt angle distribution derived from the 1917–1985 MW white-light database (see his Figure 1). The daily magnetograms used by Howard were smoothed to a resolution of $\gtrsim 3\overset{\circ}{.}4$/pixel, so

that sunspots were no longer identifiable and active regions effectively consisted entirely of plage fields. In general, as illustrated by some of the cases presented here, the trailing-polarity sectors of active regions tend to be dominated by plages, which occupy a larger area and extend to higher latitudes than the sunspots.

It is widely accepted that Joy's law has its physical origin in the Coriolis force, which acts to twist toroidally oriented flux tubes in the north–south direction as they rise buoyantly to the surface (for a dissenting view, see Kosovichev & Stenflo 2008; Stenflo & Kosovichev 2012). The tendency for the sunspot component of active regions to have a smaller axial inclination than the plage areas may then be understood as follows. As it approaches the surface, an Ω-loop expands rapidly in order to maintain pressure equilibrium with its surroundings. The expansion (or diverging flow) in the longitudinal direction, with speed $v_{\rm exp}$, gives rise to a Coriolis force ($\propto v_{\rm exp}$) that acts over a timescale $\tau_{\rm exp} \propto v_{\rm exp}^{-1}$ to produce an axial tilt $\sin\gamma \propto (v_{\rm exp}\tau_{\rm exp}^2/2)/(v_{\rm exp}\tau_{\rm exp}) \propto v_{\rm exp}^{-1}$. Since $v_{\rm exp}$ (like the buoyant velocity) scales roughly as the Alfvén speed $v_{\rm A}$, it follows that the tilt angle γ should scale inversely as the field strength B. Similar results are obtained if the limiting effects of magnetic tension and drag forces are included (see Fan et al. 1994; Fisher et al. 1995). On physical grounds, then, we would expect the tilt angles associated with sunspots to be smaller than those associated with the weaker plage fields. It should be emphasized that the axial tilt is here regarded to be a function of the local flux density, not of the area-integrated flux. Indeed, there is no clear evidence that the tilt angles of BMRs vary systematically with their total flux or areal size (Wang & Sheeley 1989, 1991; Kosovichev & Stenflo 2008; Stenflo & Kosovichev 2012), even though their spread (rms values) increase with decreasing size, an effect attributable to random displacements by supergranular convective motions (see, e.g., Howard 1989, 1996; Wang & Sheeley 1989, 1991).

5. SUMMARY AND DISCUSSION

Our main objective has been to clarify the differences between magnetic and white-light determinations of active-region tilt angles, and in particular to understand why magnetograms (used by Wang & Sheeley 1989; Howard 1991a; Tian et al. 2003; Stenflo & Kosovichev 2012; Li & Ulrich 2012) tend to yield larger inclinations than white-light images of sunspot groups (used by Howard 1991b; Dasi-Espuig et al. 2010; Ivanov 2012; McClintock & Norton 2013). Because the previous white-light studies have depended heavily on the historical MW and KK databases, we have employed the more recent DPD measurements to confirm this systematic effect and to diagnose its causes. For comparison with the white-light results, we have adopted the tilt angle measurements of Li & Ulrich (2012) as representative

of the results of magnetogram-based studies. We now summarize our conclusions (see also Tables 1 and 2).

1. When averaged over cycles 21–23 (1976–2008), the MW magnetic measurements yield larger tilt angles and Joy's law slopes than the DPD white-light observations. The mean (median) tilt angle ranges from $6\overset{\circ}{.}2\pm0\overset{\circ}{.}2$ ($7\overset{\circ}{.}5\pm0\overset{\circ}{.}2$) for MW/MAG, to $5\overset{\circ}{.}9\pm0\overset{\circ}{.}1$ ($6\overset{\circ}{.}9\pm0\overset{\circ}{.}2$) for DPD/UPP, to $5\overset{\circ}{.}3\pm0\overset{\circ}{.}2$ ($6\overset{\circ}{.}6\pm0\overset{\circ}{.}2$) for DPD/U. The mean-based (median-based) values of $m_{\rm Joy}$ are found to be 0.46±0.03 (0.52±0.03) for MW/MAG, 0.32±0.05 (0.40±0.03) for DPD/UPP, and 0.28±0.03 (0.40±0.04) for DPD/U.

2. The historical MW white-light database gives systematically smaller tilt angles and Joy's law slopes than the DPD measurements. When averaged over cycles 16–21 (1923–1985), MW/WL yields a mean (median) tilt angle of $4\overset{\circ}{.}4\pm0\overset{\circ}{.}2$ ($5\overset{\circ}{.}8\pm0\overset{\circ}{.}2$) and a mean-based (median-based) Joy's law slope of 0.20±0.01 (0.27±0.01). However, the MW and DPD data sets show surprisingly good agreement where they overlap in cycle 21 (see Figures 4–6).

3. In 43% of the MW sunspot-group measurements for cycles 16–21, the angular separation between the leading and following parts is less than $2\overset{\circ}{.}5$. In the great majority (∼84%) of these cases, as shown by Baranyi (2014), the two sectors are likely to have the same polarity. Filtering out all regions with $\Delta s < 2\overset{\circ}{.}5$ from the MW/WL and DPD/U data sets substantially increases both the average tilt angles and the Joy's law slopes. That a large fraction of the umbral-based measurements refer to "unipolar" groups reflects the tendency for well-defined sunspots to be found preferentially in the leading-polarity sectors of active regions.

4. In view of the skewed nature of the measured distributions, which are centered on positive values of γ and are thus asymmetric with respect to the imposed endpoints at $\gamma = \pm90°$, medians provide a better characterization of the tilt angle properties than simple arithmetic means (as was recognized earlier by Li & Ulrich 2012). As evident from a comparison of Tables 1 and 2, the median-based values of $m_{\rm Joy}$, γ, and $\gamma/|L|$ tend to be substantially larger than the corresponding mean-based values. It is also noteworthy that the medians change less than the means when sunspot groups with $\Delta s < 2\overset{\circ}{.}5$ are omitted.

5. That the tilt angles derived from magnetograms remain somewhat larger than those deduced from white-light images, even after filtering out unipolar sunspot groups, is due to the contribution of plages, which are seen in magnetograms but not in white light. The plage areas of an active region tend to have a larger axial inclination than the sunspots. This property was first noted by Howard (1996), although he did not correct the white-light tilt angles for the contribution of unipolar groups.

6. The difference between the sunspot and plage tilt angles can be attributed to the

action of the Coriolis force, which imparts to each buoyant flux tube a twist proportional to its rise/expansion time. Since $\tau_{\rm exp}$ scales inversely as the local field strength, the weaker, more slowly rising/expanding fields that form plages end up with a greater net twist than the stronger sunspot fields. The same holds if the twist due to the Coriolis force is limited by magnetic tension (see, e.g., Fan et al. 1994).

7. Given the large uncertainties involved in measuring tilt angles, whether white-light images or magnetograms are employed, it remains unclear whether Joy's law undergoes physically significant variations between different cycles. However, Figure 6 suggests that the cycle-averaged, latitude-normalized parameters $\gamma_{\rm mean}/|L|_{\rm mean}$ ($\sim$0.3–0.4) and $\gamma_{\rm med}/|L|_{\rm med}$ ($\sim$0.4–0.5) remain relatively constant from cycle to cycle.

Our main conclusion is that white-light measurements generally underestimate the axial inclinations of active regions, even when the leading- and following-polarity sectors are correctly identified, because the sunspot component is characterized by a smaller tilt than the plage component. By the same token, measurements employing magnetograms that underestimate the flux in sunspots (due to low spatial resolution or saturation effects) may slightly overestimate the axial tilts of active regions.

It is apparent that the tilt angles extracted from the MW white-light database do not provide a reliable basis for long-term flux-transport simulations, or for deducing cycle-to-cycle relationships among tilt angles, cycle amplitudes/total sunspot areas, and the polar fields (see Dasi-Espuig et al. 2010; Muñoz-Jaramillo et al. 2013). However, these measurements could be improved by exploiting the polarity information available in the daily MW sunspot-group drawings. In addition, use should be made of the digitized MW Ca II K-line images spanning the period 1915–1985,[6] which show the plage areas associated with the sunspot groups, while at the same time outlining more clearly the boundaries of the active regions (see, e.g., Figures 1 to 12 in Sheeley et al. 2011). It would be particularly instructive to compare the tilt angles defined by the Ca II emission contours with those derived from the white-light sunspots.

From an analysis of white-light facular data compiled by the Royal Greenwich Observatory, Foukal (1993) concluded that the ratio of facular to sunspot area decreased during the highest-amplitude cycles (18 and 19). Since faculae are the white-light counterparts (visible near the limb) of plages and strong magnetic network, such a decrease would imply that the axial tilts of active regions should be somewhat smaller during very active cycles than in weaker cycles. However, recent photometric measurements by Chapman et al. (2011) indicate that the facular/plage area in fact increases linearly with sunspot area, without

[6]See `http://ulrich.astro.ucla.edu/MW_SPADP`.

flattening out for large total sunspot areas.

An important question not addressed in this study is the effect of evolutionary processes on the measured tilt angles. That the values obtained depend on when the measurements are made was already emphasized by Brunner (1930), who noted that the axial inclinations of emerging sunspot groups decrease with time due to the westward proper motions of their leading spots (see also Kosovichev & Stenflo 2008). The slope derived for Joy's law depends sensitively on the relatively few active regions at latitudes $|L| \gtrsim 25°$, which are also those most strongly affected by differential rotation. For a BMR centered at $|L| = 27.^{\circ}5$ with a latitudinal pole separation of 2°, for example, $\Delta\phi$ increases at a rate of $\sim 0.^{\circ}09$ day^{-1}, so that rotational shearing may have a noticeable effect on the inclinations of regions older than ∼10 days. Tilt angle measurements should also be performed before supergranular diffusion has converted the sunspot fields into network/plage.

It is clear from this study that reliable and physically meaningful tilt angles cannot be derived from white-light images alone, which not only lack the essential polarity information, but also omit the plage component of active regions. Even when magnetograms are employed, care is needed when applying automated techniques. Ideally, each active region should be tracked from day to day and its axial inclination measured at the time of peak development, after the flux has fully emerged but before it begins to decay through transport processes. Such tracking, which also makes it easier to identify the boundaries of closely spaced active regions, is probably best done by human eye; a computer algorithm can then be employed to determine the centroids of the leading- and trailing-polarity flux within the visually checked/adjusted active-region boundaries.

It will be especially interesting to compare the magnetic tilt angles determined for the current weak cycle with those derived for cycles 21–23. Accurate measurements using a combination of visual and automated techniques may help to resolve the question of whether cycle-to-cycle variations in the polar fields are related to systematic variations in the axial tilts of active regions.

We thank the referee for comments, and G. Chintzoglou, J. S. Morrill, K. Muglach, N. R. Sheeley, Jr., D. G. Socker, R. K. Ulrich, and the participants of the International Space Science Institute Workshop on "The Solar Activity Cycle: Physical Causes and Consequences" for helpful discussions. We are also indebted to the Debrecen Heliophysical Observatory, MW/UCLA, and NSO/KP for providing the data used in this investigation, which was funded by the Office of Naval Research and by the European Community's Seventh Framework Programme (project eHEROES).

REFERENCES

Babcock, H. D. 1959, ApJ, 130, 364

Baranyi, T. 2014, MNRAS, submitted

Baumann, I., Schmitt, D., Schüssler, M., & Solanki, S. K. 2004, A&A, 426, 1075

Brunner, W. 1930, MiZur, 124, 67

Caligari, P., Moreno-Insertis, F., & Schüssler, M. 1995, ApJ, 441, 886

Cameron, R. H., Jiang, J., Schmitt, D., & Schüssler, M. 2010, ApJ, 719, 264

Cameron, R. H., & Schüssler, M. 2012, A&A, 548, A57

Chapman, G. A., Dobias, J. J., & Arias, T. 2011, ApJ, 728, 150

Dasi-Espuig, M., Solanki, S. K., Krivova, N. A., Cameron, R., & Peñuela, T. 2010, A&A, 518, A7

Dasi-Espuig, M., Solanki, S. K., Krivova, N. A., Cameron, R., & Peñuela, T. 2013, A&A, 556, C3

Dikpati, M., & Charbonneau, P. 1999, ApJ, 518, 508

D'Silva, S., & Choudhuri, A. R. 1993, A&A, 272, 621

Fan, Y., Fisher, G. H., & DeLuca, E. E. 1993, ApJ, 405, 390

Fan, Y., Fisher, G. H., & McClymont, A. N. 1994, ApJ, 436, 907

Fisher, G. H., Fan, Y., & Howard, R. F. 1995, ApJ, 438, 463

Foukal, P. 1993, SoPh, 148, 219

Győri, L., Baranyi, T., & Ludmány, A. 2011, The Physics of Sun and Star Spots (IAU Symp. 273), ed. D. P. Choudhary & K. G. Strassmeier (Cambridge: Cambridge Univ. Press), 403

Hale, G. E., Ellerman, F., Nicholson, S. B., & Joy, A. H. 1919, ApJ, 49, 153

Hathaway, D. H., & Upton, L. 2014, JGR, 119, 3316

Howard, R. F. 1989, SoPh, 123, 271

Howard, R. F. 1991a, SoPh, 132, 49

Howard, R. F. 1991b, SoPh, 136, 251

Howard, R. F. 1996, SoPh, 169, 293

Howard, R., Gilman, P. A., & Gilman, P. I. 1984, ApJ, 283, 373

Ivanov, V. G. 2012, Ge&Ae, 52, 999

Jiang, J., Cameron, R. H., Schmitt, D., & Işik, E. 2013, A&A, 553, A128

Jiang, J., Cameron, R. H., Schmitt, D., & Schüssler, M. 2011a, A&A, 528, A82

Jiang, J., Cameron, R. H., Schmitt, D., & Schüssler, M. 2011b, A&A, 528, A83

Jiang, J., Cameron, R. H., & Schüssler, M. 2014, ApJ, 791, 5

Kitchatinov, L. L., & Olemskoy, S. V. 2011, AstL, 37, 656

Kosovichev, A. G., & Stenflo, J. O. 2008, ApJ, 688, L115

Li, J., & Ulrich, R. K. 2012, ApJ, 758, 115

Mackay, D. H., Priest, E. R., & Lockwood, M. 2002, SoPh, 207, 291

McClintock, B. H., & Norton, A. A. 2013, SoPh, 287, 215

Muñoz-Jaramillo, A., Dasi-Espuig, M., Balmaceda, L. A., & DeLuca, E. E. 2013, ApJ, 767, L25

Muñoz-Jaramillo, A., Nandy, D., Martens, P. C. H., & Yeates, A. R. 2010, ApJ, 720, L20

Muraközy, J., Baranyi, T., & Ludmány, A. 2014, SoPh, 289, 563

Schrijver, C. J. 1987, A&A, 180, 241

Schüssler, M., & Baumann, I. 2006, A&A, 459, 945

Sheeley, N. R., Jr. 1966, ApJ, 144, 723

Sheeley, N. R., Jr. 2008, ApJ, 680, 1553

Sheeley, N. R., Jr., Cooper, T. J., & Anderson, J. R. L. 2011, ApJ, 730, 51

Stenflo, J. O., & Kosovichev, A. G. 2012, ApJ, 745, 129

Tian, L., Liu, Y., & Wang, H. 2003, SoPh, 215, 281

Tlatov, A. G., Tlatova, K. A., Vasil'eva, V. V., Pevtsov, A. A., & Mursula, K. 2014, AdSpR, in press

Upton, L., & Hathaway, D. H. 2014a, ApJ, 780, 5

Upton, L., & Hathaway, D. H. 2014b, ApJ, 792, 142

Wang, Y.-M., & Sheeley, N. R., Jr. 1989, SoPh, 124, 81

Wang, Y.-M., & Sheeley, N. R., Jr. 1991, ApJ, 375, 761

Table 1. Tilt Angle Parameters (Mean-Based)

		Cycle Number									
Parameter	Database	16	17	18	19	20	21	22	23	16–21	21–23
$m_{\rm Joy}^{\rm (mean)}$	MW/MAG	···	···	···	···	···	0.48±0.05	0.37±0.07	0.50±0.06	···	0.46±0.03
	($\Delta s > 2\overset{\circ}{.}5$)	···	···	···	···	···	0.47±0.03	0.42±0.06	0.53±0.07	···	0.48±0.04
	MW/WL	0.28±0.11	0.17±0.05	0.21±0.08	0.19±0.02	0.14±0.04	0.27±0.06	···	···	0.20±0.01	···
	($\Delta s > 2\overset{\circ}{.}5$)	0.51±0.12	0.43±0.08	0.20±0.02	0.27±0.06	0.36±0.04	0.34±0.08	···	···	0.32±0.04	···
	DPD/U	···	···	···	···	···	0.16±0.06	0.36±0.05	0.33±0.08	···	0.28±0.03
	($\Delta s > 2\overset{\circ}{.}5$)	···	···	···	···	···	0.31±0.02	0.47±0.05	0.43±0.05	···	0.40±0.03
	DPD/UPP	···	···	···	···	···	0.27±0.07	0.32±0.04	0.38±0.05	···	0.32±0.05
	($\Delta s > 2\overset{\circ}{.}5$)	···	···	···	···	···	0.28±0.05	0.37±0.04	0.41±0.03	···	0.35±0.04
$\gamma_{\rm mean}$	MW/MAG	···	···	···	···	···	$5\overset{\circ}{.}8\pm0\overset{\circ}{.}3$	$6\overset{\circ}{.}8\pm0\overset{\circ}{.}3$	$6\overset{\circ}{.}1\pm0\overset{\circ}{.}3$	···	$6\overset{\circ}{.}2\pm0\overset{\circ}{.}2$
	($\Delta s > 2\overset{\circ}{.}5$)	···	···	···	···	···	$6\overset{\circ}{.}0\pm0\overset{\circ}{.}3$	$7\overset{\circ}{.}0\pm0\overset{\circ}{.}3$	$6\overset{\circ}{.}3\pm0\overset{\circ}{.}3$	···	$6\overset{\circ}{.}4\pm0\overset{\circ}{.}2$
	MW/WL	$4\overset{\circ}{.}4\pm0\overset{\circ}{.}6$	$4\overset{\circ}{.}7\pm0\overset{\circ}{.}5$	$4\overset{\circ}{.}8\pm0\overset{\circ}{.}5$	$3\overset{\circ}{.}6\pm0\overset{\circ}{.}4$	$4\overset{\circ}{.}1\pm0\overset{\circ}{.}5$	$5\overset{\circ}{.}3\pm0\overset{\circ}{.}5$	···	···	$4\overset{\circ}{.}4\pm0\overset{\circ}{.}2$	···
	($\Delta s > 2\overset{\circ}{.}5$)	$6\overset{\circ}{.}6\pm0\overset{\circ}{.}5$	$5\overset{\circ}{.}5\pm0\overset{\circ}{.}5$	$6\overset{\circ}{.}4\pm0\overset{\circ}{.}4$	$4\overset{\circ}{.}6\pm0\overset{\circ}{.}4$	$5\overset{\circ}{.}5\pm0\overset{\circ}{.}4$	$6\overset{\circ}{.}4\pm0\overset{\circ}{.}5$	···	···	$5\overset{\circ}{.}8\pm0\overset{\circ}{.}2$	···
	DPD/U	···	···	···	···	···	$5\overset{\circ}{.}2\pm0\overset{\circ}{.}3$	$5\overset{\circ}{.}1\pm0\overset{\circ}{.}3$	$5\overset{\circ}{.}6\pm0\overset{\circ}{.}3$	···	$5\overset{\circ}{.}3\pm0\overset{\circ}{.}2$
	($\Delta s > 2\overset{\circ}{.}5$)	···	···	···	···	···	$6\overset{\circ}{.}6\pm0\overset{\circ}{.}3$	$6\overset{\circ}{.}2\pm0\overset{\circ}{.}2$	$6\overset{\circ}{.}4\pm0\overset{\circ}{.}2$	···	$6\overset{\circ}{.}4\pm0\overset{\circ}{.}1$
	DPD/UPP	···	···	···	···	···	$5\overset{\circ}{.}5\pm0\overset{\circ}{.}2$	$6\overset{\circ}{.}1\pm0\overset{\circ}{.}2$	$6\overset{\circ}{.}3\pm0\overset{\circ}{.}2$	···	$5\overset{\circ}{.}9\pm0\overset{\circ}{.}1$
	($\Delta s > 2\overset{\circ}{.}5$)	···	···	···	···	···	$6\overset{\circ}{.}1\pm0\overset{\circ}{.}2$	$6\overset{\circ}{.}7\pm0\overset{\circ}{.}2$	$7\overset{\circ}{.}0\pm0\overset{\circ}{.}2$	···	$6\overset{\circ}{.}6\pm0\overset{\circ}{.}1$
$\gamma_{\rm mean}/\lvert L\rvert_{\rm mean}$	MW/MAG	···	···	···	···	···	0.37±0.02	0.41±0.02	0.39±0.02	···	0.39±0.01
	($\Delta s > 2\overset{\circ}{.}5$)	···	···	···	···	···	0.38±0.02	0.42±0.02	0.40±0.02	···	0.40±0.01
	MW/WL	0.31±0.04	0.32±0.04	0.32±0.03	0.22±0.02	0.29±0.03	0.35±0.03	···	···	0.29±0.01	···
	($\Delta s > 2\overset{\circ}{.}5$)	0.46±0.04	0.38±0.03	0.43±0.03	0.28±0.02	0.40±0.03	0.43±0.03	···	···	0.38±0.01	···
	DPD/U	···	···	···	···	···	0.33±0.02	0.31±0.02	0.36±0.02	···	0.33±0.01
	($\Delta s > 2\overset{\circ}{.}5$)	···	···	···	···	···	0.42±0.02	0.37±0.01	0.40±0.02	···	0.40±0.01
	DPD/UPP	···	···	···	···	···	0.35±0.01	0.37±0.01	0.40±0.01	···	0.37±0.01
	($\Delta s > 2\overset{\circ}{.}5$)	···	···	···	···	···	0.39±0.01	0.41±0.01	0.45±0.01	···	0.42±0.01

Note. — Here and throughout this study, only measurements made within 45° of central meridian longitude are included in the statistics. Quoted errors, based on the number of measurements and their scatter, are 1σ; the actual uncertainties are probably much larger. The MW/WL and DPD/U tilt angles are derived from the area-weighted positions of umbrae only, while the DPD/UPP measurements include umbrae, penumbrae, and faint pores. The second row of values provided for each database shows the result of omitting all regions whose leading and following centroids are separated by less than $2\overset{\circ}{.}5$ (see text). Cycle dates are: 1923 August–1933 August (16), 1933 September–1944 January (17), 1944 February–1954 March (18), 1954 April–1964 September (19), 1964 October–1976 May (20), 1976 June–1986 August (21), 1986 September–1996 April (22), 1996 May–2008 December (23).

Table 2. Tilt Angle Parameters (Median-Based)

		Cycle Number									
Parameter	Database	16	17	18	19	20	21	22	23	16–21	21–23
$m_{\rm Joy}^{\rm (med)}$	MW/MAG	···	···	···	···	···	0.57±0.03	0.47±0.05	0.48±0.05	···	0.52±0.03
	($\Delta s > 2.^\circ5$)	···	···	···	···	···	0.57±0.03	0.51±0.04	0.49±0.05	···	0.53±0.03
	MW/WL	0.41±0.12	0.30±0.02	0.14±0.09	0.24±0.05	0.21±0.07	0.41±0.06	···	···	0.27±0.01	···
	($\Delta s > 2.^\circ5$)	0.47±0.14	0.46±0.08	0.16±0.02	0.29±0.07	0.37±0.06	0.45±0.08	···	···	0.34±0.04	···
	DPD/U	···	···	···	···	···	0.34±0.02	0.46±0.06	0.41±0.06	···	0.40±0.04
	($\Delta s > 2.^\circ5$)	···	···	···	···	···	0.41±0.04	0.50±0.06	0.46±0.04	···	0.45±0.04
	DPD/UPP	···	···	···	···	···	0.36±0.03	0.37±0.05	0.44±0.04	···	0.40±0.03
	($\Delta s > 2.^\circ5$)	···	···	···	···	···	0.38±0.04	0.35±0.04	0.44±0.02	···	0.40±0.03
$\gamma_{\rm med}$	MW/MAG	···	···	···	···	···	$7.^\circ5\pm0.^\circ4$	$7.^\circ8\pm0.^\circ4$	$7.^\circ1\pm0.^\circ3$	···	$7.^\circ5\pm0.^\circ2$
	($\Delta s > 2.^\circ5$)	···	···	···	···	···	$7.^\circ55\pm0.^\circ4$	$7.^\circ8\pm0.^\circ4$	$7.^\circ1\pm0.^\circ3$	···	$7.^\circ5\pm0.^\circ2$
	MW/WL	$6.^\circ1\pm0.^\circ7$	$5.^\circ3\pm0.^\circ7$	$6.^\circ4\pm0.^\circ6$	$4.^\circ7\pm0.^\circ5$	$5.^\circ5\pm0.^\circ6$	$7.^\circ4\pm0.^\circ6$	···	···	$5.^\circ8\pm0.^\circ2$	···
	($\Delta s > 2.^\circ5$)	$7.^\circ4\pm0.^\circ7$	$5.^\circ85\pm0.^\circ6$	$7.^\circ4\pm0.^\circ5$	$5.^\circ1\pm0.^\circ5$	$5.^\circ8\pm0.^\circ5$	$7.^\circ8\pm0.^\circ6$	···	···	$6.^\circ4\pm0.^\circ2$	···
	DPD/U	···	···	···	···	···	$6.^\circ7\pm0.^\circ4$	$6.^\circ0\pm0.^\circ4$	$7.^\circ0\pm0.^\circ4$	···	$6.^\circ6\pm0.^\circ2$
	($\Delta s > 2.^\circ5$)	···	···	···	···	···	$7.^\circ2\pm0.^\circ3$	$6.^\circ4\pm0.^\circ3$	$7.^\circ25\pm0.^\circ3$	···	$7.^\circ0\pm0.^\circ2$
	DPD/UPP	···	···	···	···	···	$6.^\circ8\pm0.^\circ3$	$6.^\circ5\pm0.^\circ3$	$7.^\circ4\pm0.^\circ3$	···	$6.^\circ9\pm0.^\circ2$
	($\Delta s > 2.^\circ5$)	···	···	···	···	···	$7.^\circ2\pm0.^\circ3$	$6.^\circ9\pm0.^\circ3$	$7.^\circ8\pm0.^\circ3$	···	$7.^\circ3\pm0.^\circ2$
$\gamma_{\rm med}/\lvert L\rvert_{\rm med}$	MW/MAG	···	···	···	···	···	0.50±0.02	0.48±0.02	0.48±0.02	···	0.48±0.01
	($\Delta s > 2.^\circ5$)	···	···	···	···	···	0.49±0.02	0.48±0.02	0.48±0.02	···	0.48±0.01
	MW/WL	0.44±0.05	0.38±0.05	0.44±0.04	0.30±0.03	0.41±0.04	0.51±0.04	···	···	0.40±0.02	···
	($\Delta s > 2.^\circ5$)	0.53±0.05	0.43±0.04	0.53±0.04	0.32±0.03	0.44±0.04	0.54±0.04	···	···	0.45±0.02	···
	DPD/U	···	···	···	···	···	0.45±0.03	0.38±0.02	0.47±0.02	···	0.43±0.01
	($\Delta s > 2.^\circ5$)	···	···	···	···	···	0.48±0.02	0.40±0.02	0.47±0.02	···	0.45±0.01
	DPD/UPP	···	···	···	···	···	0.45±0.02	0.41±0.02	0.49±0.02	···	0.45±0.01
	($\Delta s > 2.^\circ5$)	···	···	···	···	···	0.48±0.02	0.44±0.02	0.51±0.02	···	0.48±0.01

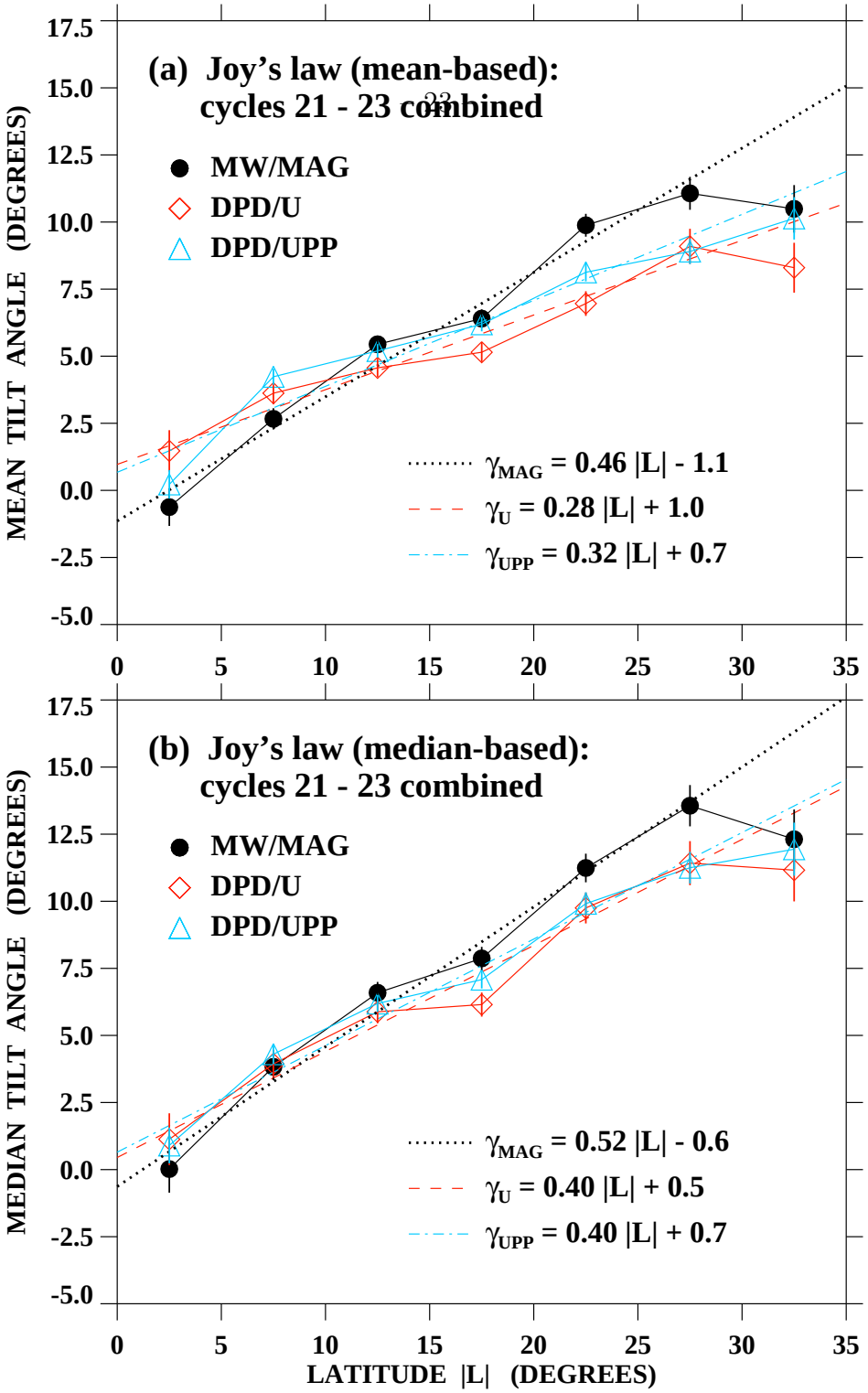

Fig. 1.— Joy's law for cycles 21–23 combined, derived from the MW magnetic measurements of Li & Ulrich (2012: MW/MAG), and from Debrecen Observatory white-light measurements based on dark umbrae only (DPD/U) and on umbrae, penumbrae, and pores (DPD/UPP). (a) Mean-based Joy's law: arithmetic means of the tilt angle measurements have been taken over 5°-wide bins in unsigned latitude $|L|$, and a least-squares linear fit applied to the six points spanning the range 0°–30°. Vertical bars indicate one standard error of the mean. (b) Median-based Joy's law: here, median values of the measured tilt angles have been calculated for each latitude bin and a least-squares fit applied over the range 0°–30°. Vertical bars represent one standard error of the median.

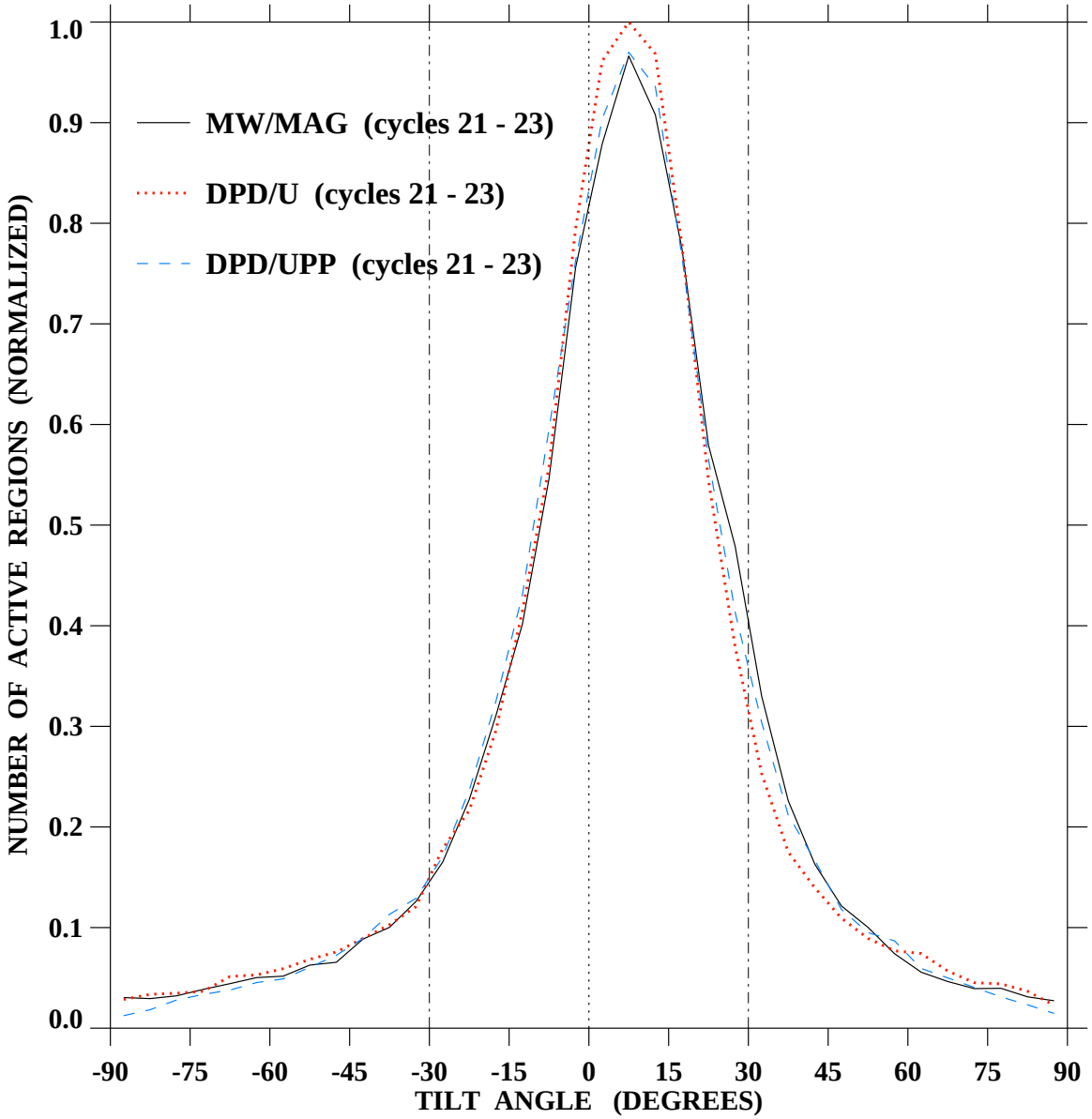

Fig. 2.— Histograms (frequency distributions) of active-region tilt angles measured during 1976–2008 (cycles 21–23), normalized by dividing by the total number of measurements in each data set and multiplying by an arbitrary constant. Black solid curve: MW/MAG (HWHM = 17.°5). Red dotted curve: DPD/U (HWHM = 15.°4). Blue dashed curve: DPD/UPP (HWHM = 16.°9). Bin size for the histograms is 5° (the discrete bin points are connected by a smooth curve rather than being plotted in steplike fashion). Vertical dotted (dash-dotted) lines mark the location of $\gamma = 0°$ ($\gamma = \pm 30°$). Significant differences between the three Gaussian-like distributions occur over the interval $+25° \lesssim \gamma \lesssim +40°$, with DPD/UPP and especially MW/MAG showing a greater relative number of these large tilt angles than DPD/U, which makes up for its deficit with a surplus at small tilt angles. The restriction of γ to the range between $-90°$ and $+90°$ causes the distribution functions to be skewed leftward relative to their peaks, which in turn explains why their means are smaller than their medians.

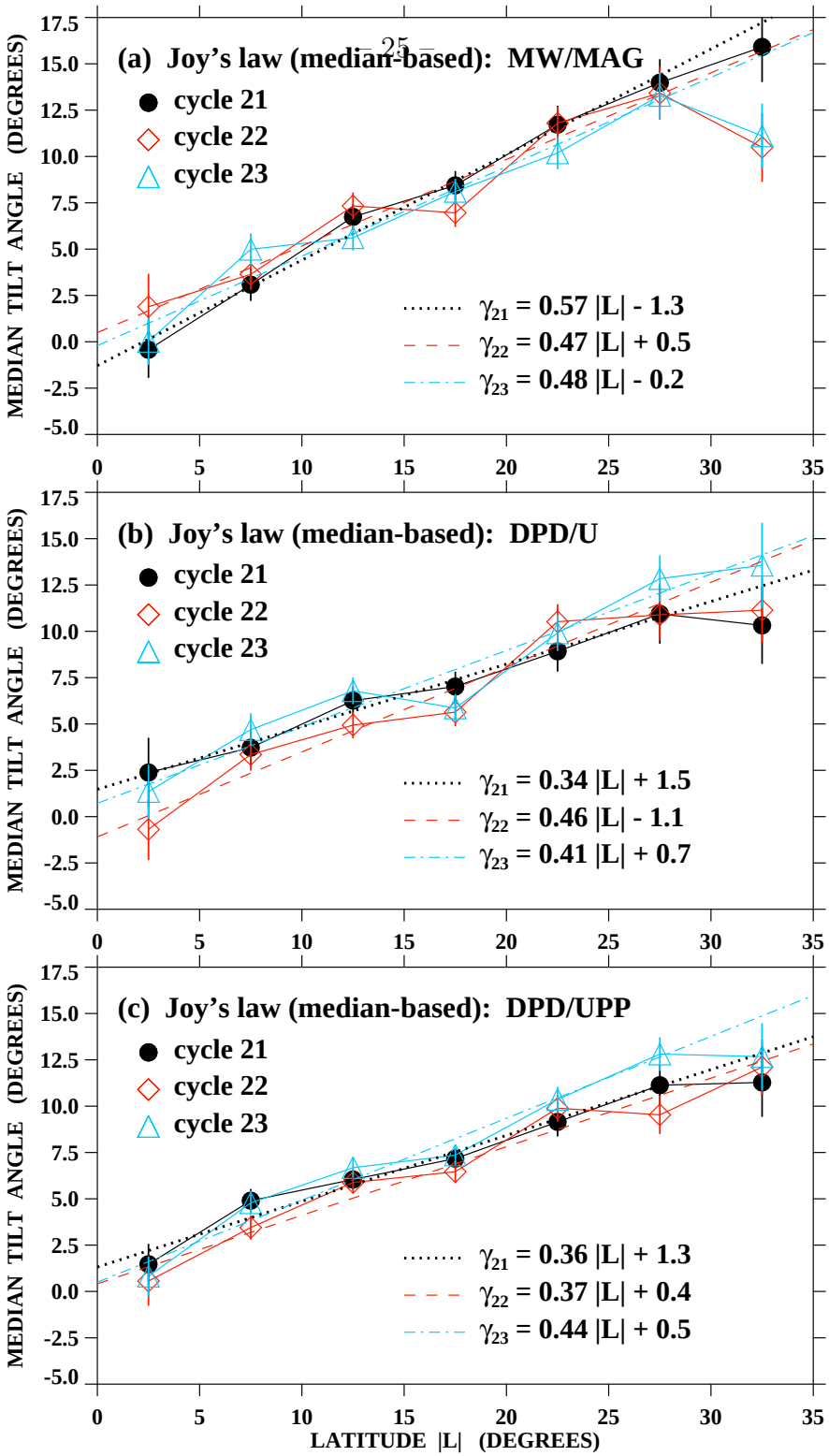

Fig. 3.— Median-based Joy's law derived separately for cycle 21 (1976 June–1986 August), cycle 22 (1986 September–1996 April), and cycle 23 (1996 May–2008 December). (a) MW/MAG measurements (Li & Ulrich 2012). (b) DPD/U white-light measurements (including dark umbrae only). (c) DPD/UPP white-light measurements (including umbrae, penumbrae, and faint pores).

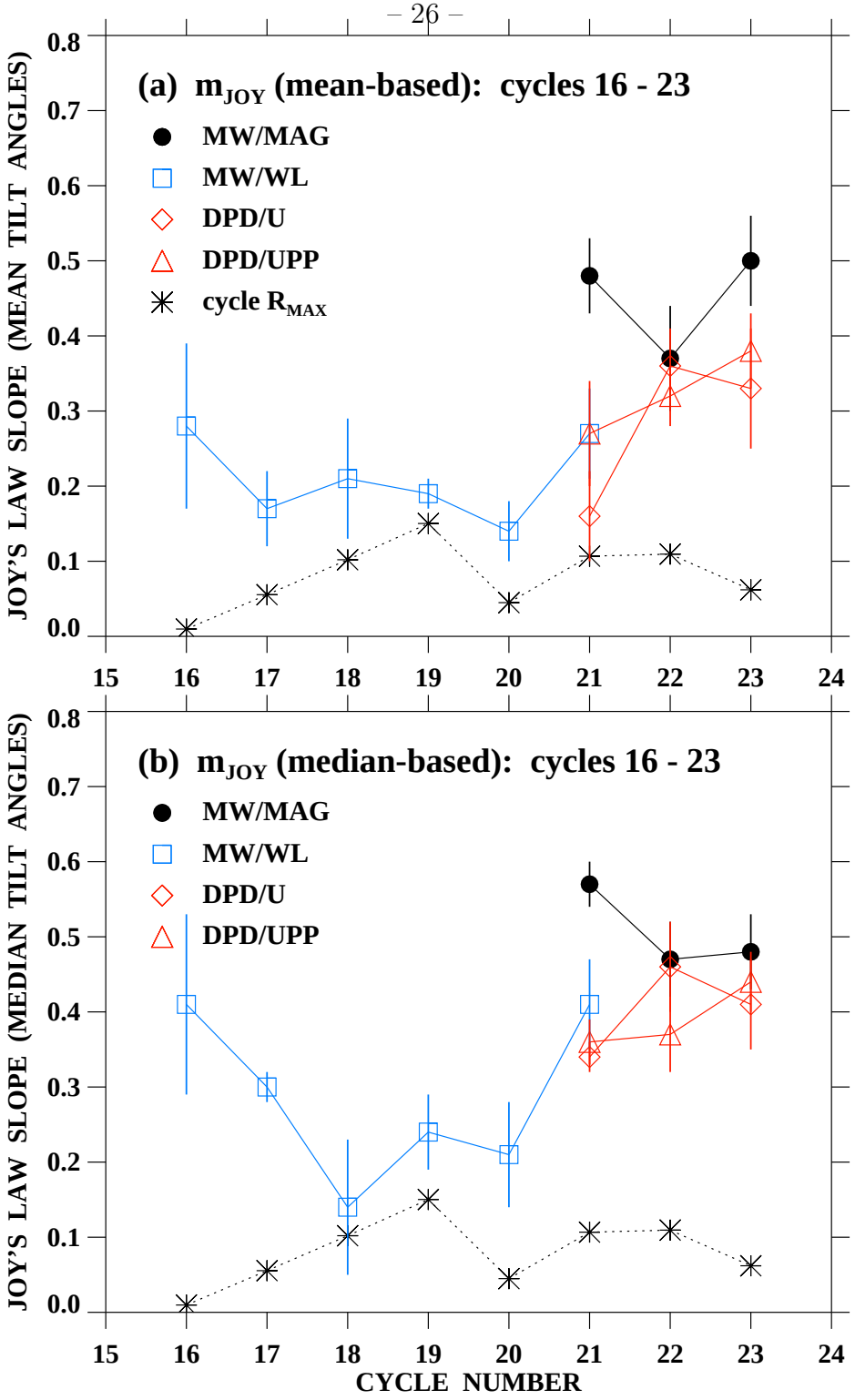

Fig. 4.— Cycle-averaged Joy's law slopes, derived from MW/MAG, MW/WL, DPD/U, and DPD/UPP measurements. (a) Mean-based values $m_{\rm Joy}^{\rm (mean)}$. (b) Median-based values $m_{\rm Joy}^{\rm (med)}$. Vertical bars show 1σ errors. Asterisks indicate the (arbitrarily shifted and scaled) maximum yearly sunspot numbers $R_{\rm max}$ for cycles 16–23.

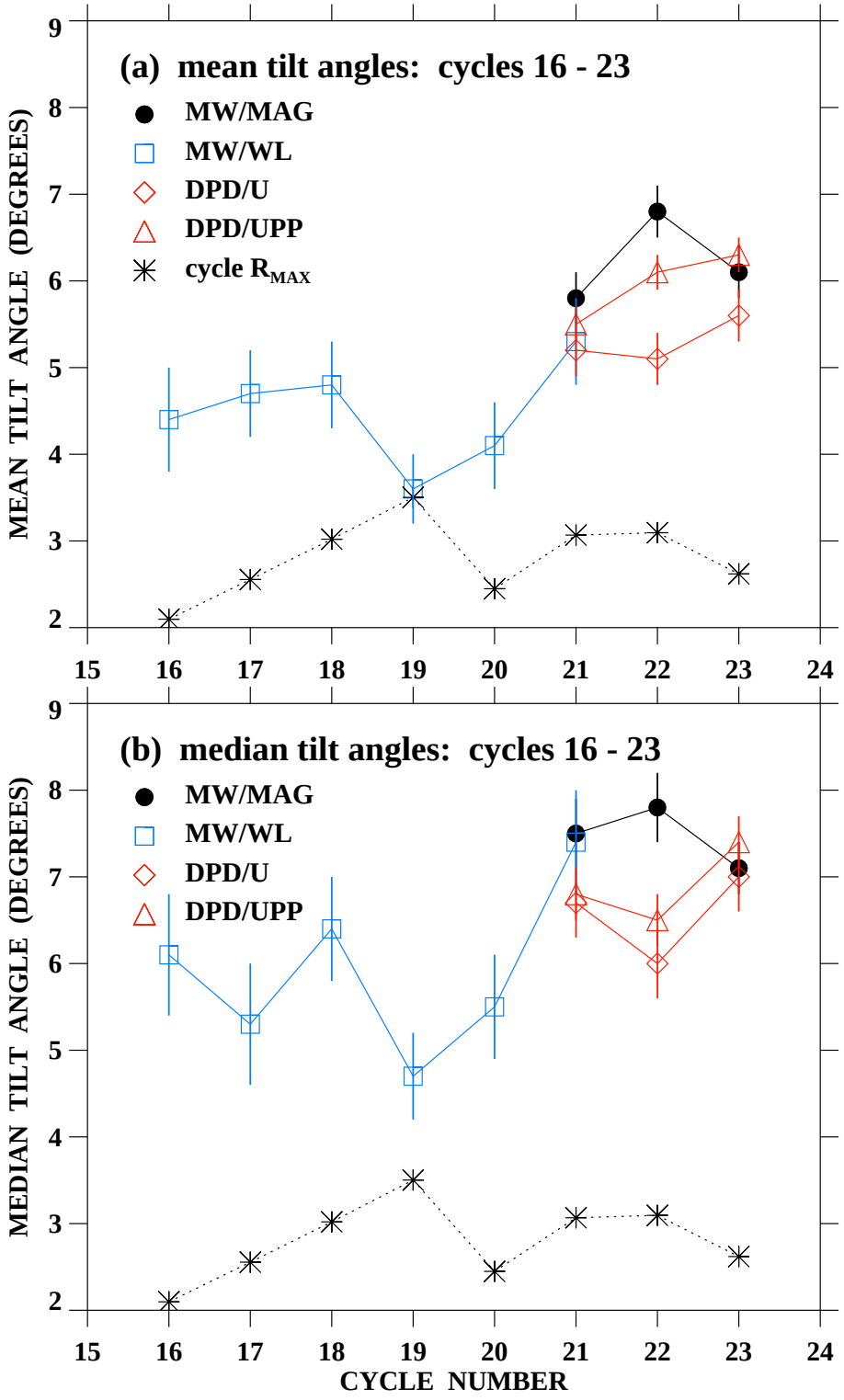

Fig. 5.— Cycle-averaged tilt angles derived from MW/MAG, MW/WL, DPD/U, and DPD/UPP measurements. (a) Mean values $\gamma_{\rm mean}$. (b) Median values $\gamma_{\rm med}$.

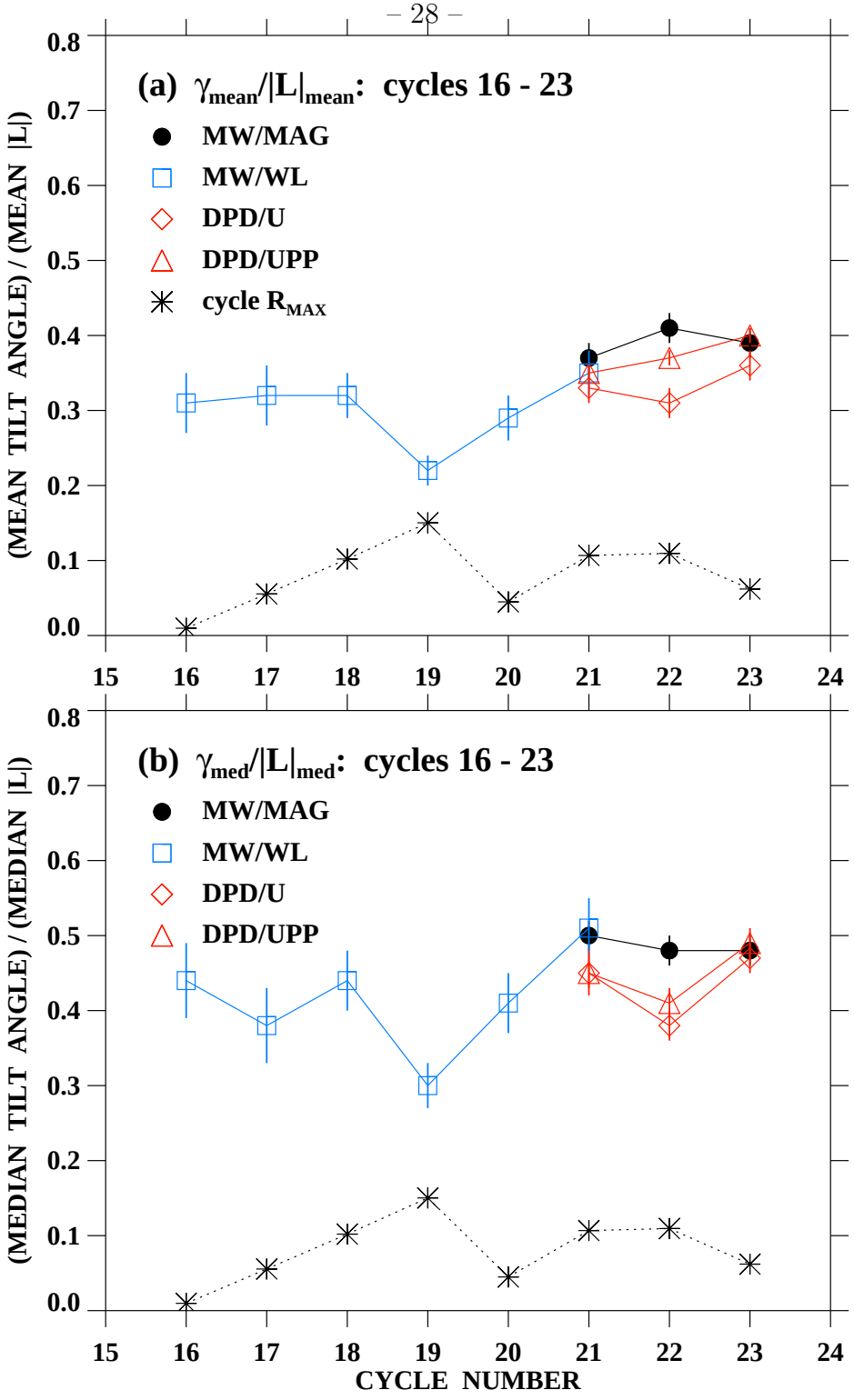

Fig. 6.— Ratio of cycle-averaged tilt angle to cycle-averaged latitude, derived from MW/MAG, MW/WL, DPD/U, and DPD/UPP measurements. (a) $\gamma_{\rm mean}/|L|_{\rm mean}$. (b) $\gamma_{\rm med}/|L|_{\rm med}$. Normalizing by latitude reduces both the cycle-to-cycle variation and the spread between the different data sets.

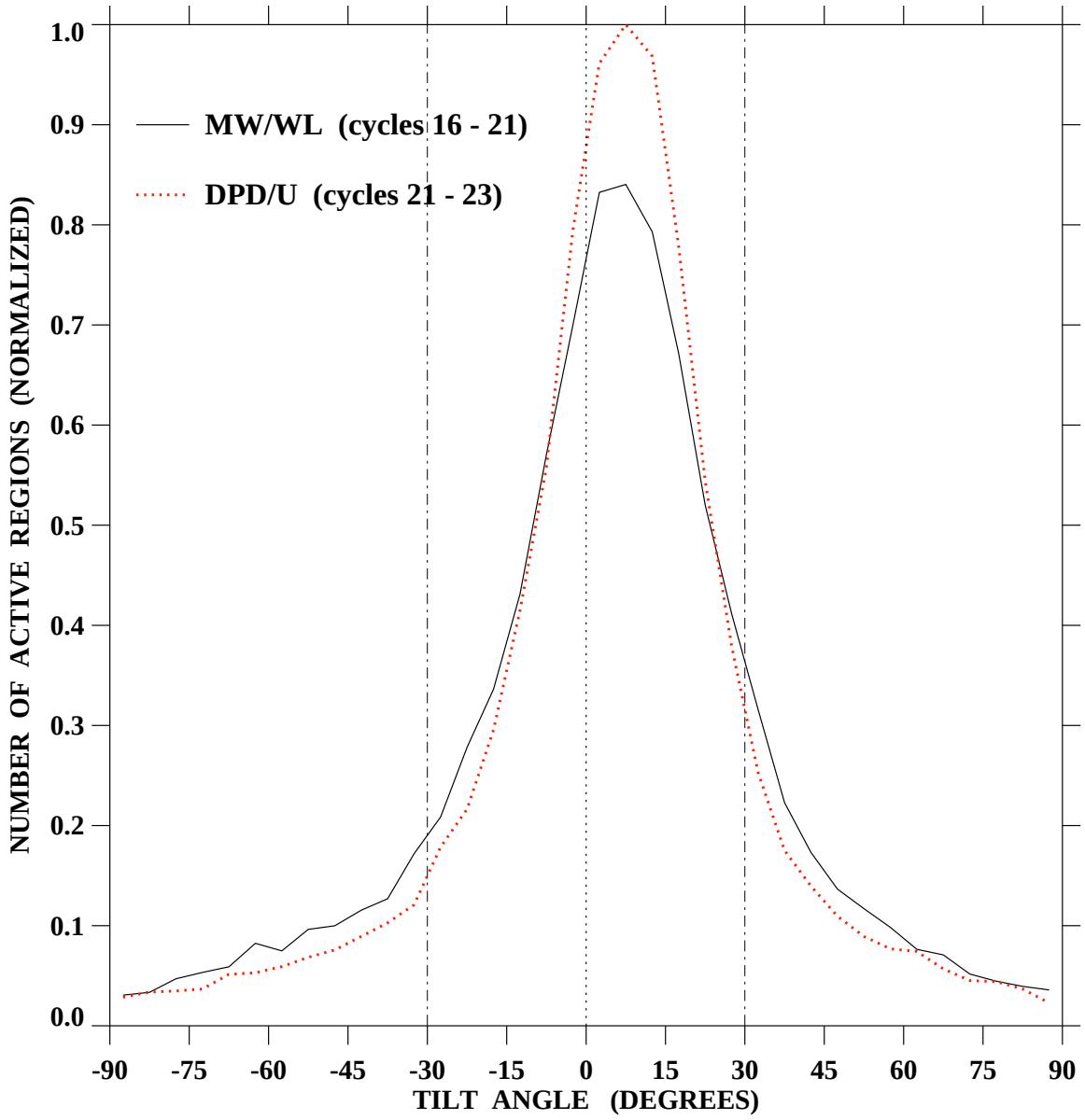

Fig. 7.— Frequency distribution of MW/WL tilt angles measured for cycles 16–21 (black solid curve), displayed together with the corresponding DPD/U histogram for cycles 21–23 (red dotted curve). Both histograms (bin width 5°) have been normalized by dividing by the total number of measurements in each data set and multiplying by an arbitrary constant. The MW/WL distribution has HWHM = 17.°9, and shows a larger frequency of both positive and negative outliers than DPD/U (HWHM = 15.°4).

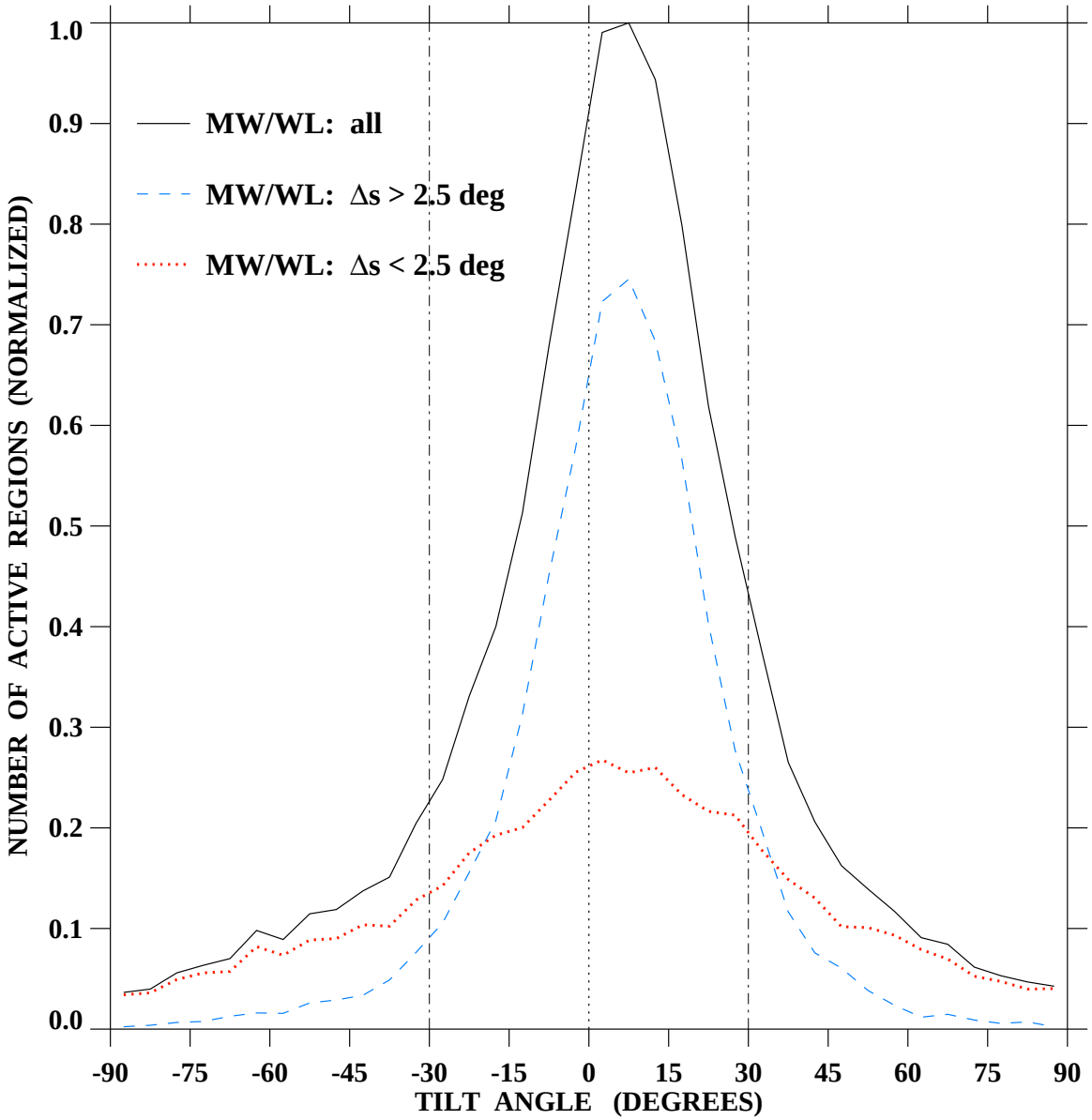

Fig. 8.— The histogram of MW/WL tilt angles measured for cycles 16–21 (black solid curve) is here separated into a component consisting of 12,777 sunspot groups with angular separations $\Delta s > 2.^\circ5$ (blue dashed curve), and a component consisting of the remaining 9756 sunspot groups with $\Delta s < 2.^\circ5$ (red dotted curve). All three histograms have bin width 5° and have been normalized by dividing by the total number of MW/WL measurements (22,533) and multiplying by a constant scaling factor. The tilt angle distribution of sunspot groups with $\Delta s < 2.^\circ5$, the great majority of which have leading and following sectors of the same polarity, is extremely broad (HWHM = $25.^\circ7$). Filtering out this component reduces the HWHM of the original distribution from $17.^\circ9$ to $16.^\circ6$, and removes most of the outliers in the far wings.

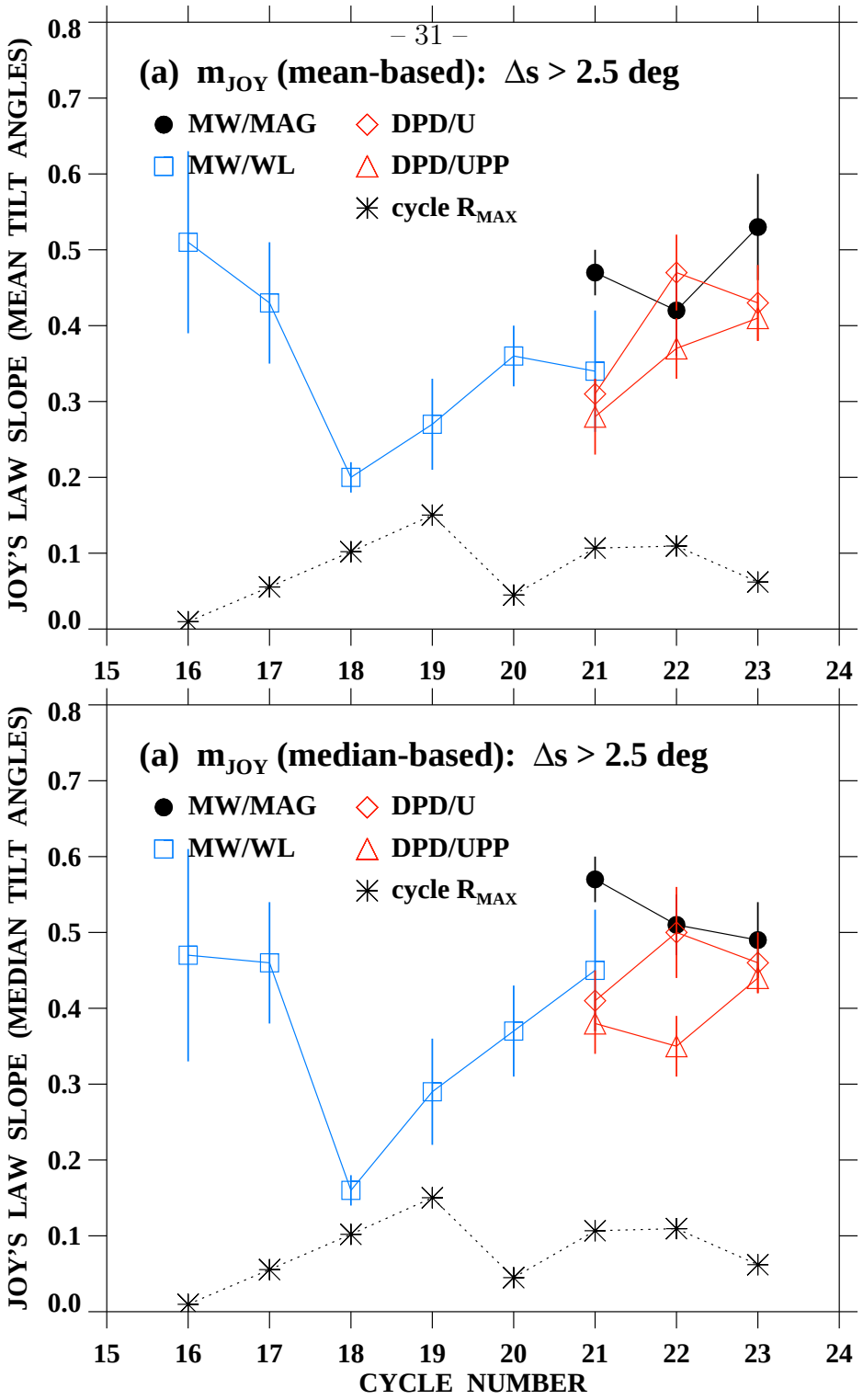

Fig. 9.— Cycle-averaged Joy's law slopes derived from MW/MAG, MW/WL, DPD/U, and DPD/UPP measurements, after omitting active regions with angular separations $\Delta s < 2.^{\circ}5$. (a) Mean values. (b) Median values. Compare Figure 4, where all active regions are included in the averages. The filtering condition removes most of the "unipolar" sunspot groups from the MW/WL and DPD data sets.

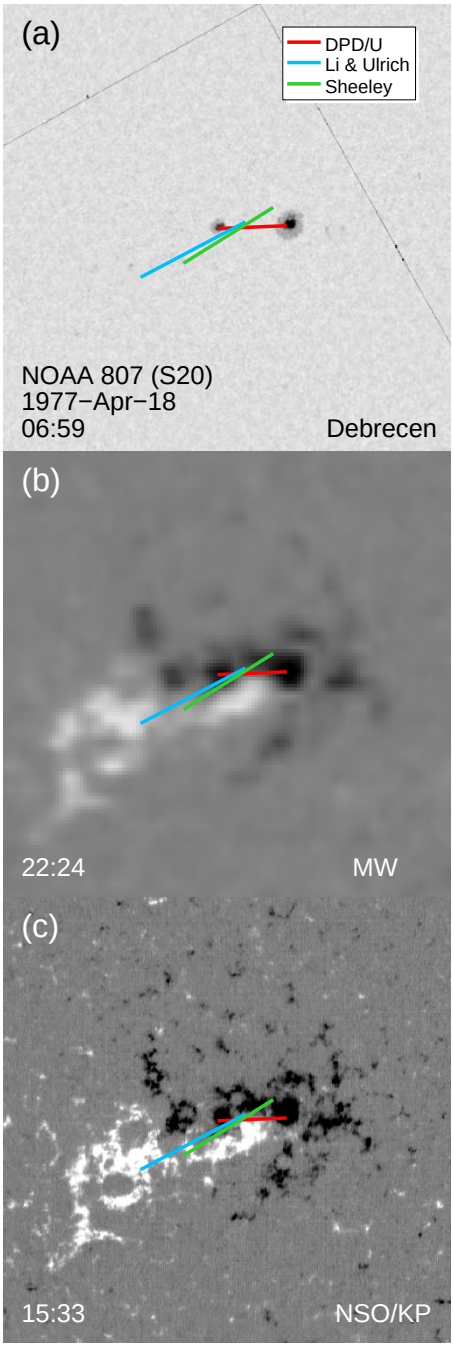

Fig. 10.— Comparison of white-light and magnetic tilt-angle measurements for NOAA 807, centered at $L \simeq -20°$. (a) White-light image taken by the Debrecen Observatory at 06:59 UT on 1977 April 18. (b) MW magnetogram recorded at 22:24 UT. (c) NSO/KP magnetogram recorded at 15:33 UT. Colored lines overplotted on each image connect the measured centroids (corrected for differential rotation) of the leading and following sectors. Red: DPD/U ($\gamma = 2\overset{\circ}{.}5$). Blue: MW/MAG ($\gamma = 29\overset{\circ}{.}8$; see Li & Ulrich 2012). Green: KP/MAG ($\gamma = 29\overset{\circ}{.}7$; see Wang & Sheeley 1989). The white-light image is dominated by a pair of sunspots separated by $4\overset{\circ}{.}5$; DPD/U assigns the easternmost spot to the following sector, even though the magnetograms show that it has the leading polarity. The resulting γ is much smaller than that obtained from the magnetic measurements. This active region also provides an example of longitudinal overlap between leading- and trailing-polarity sectors, another major source of error in white-light tilt-angle determinations (see also Figure 12).

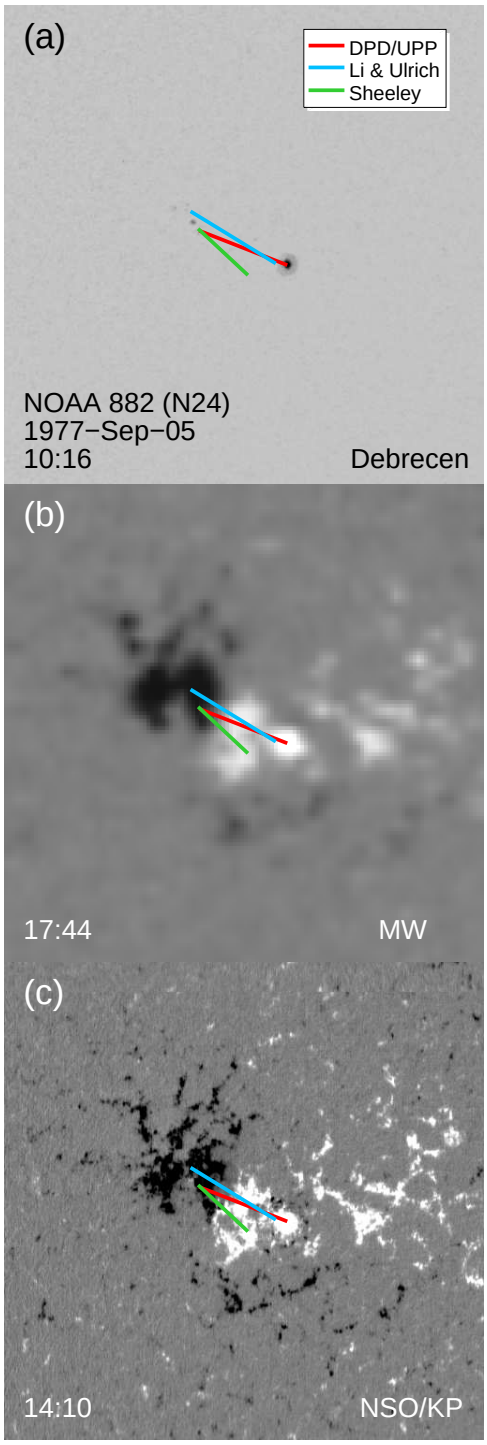

Fig. 11.— Comparison of white-light and magnetic tilt-angle measurements for NOAA 882, centered at $L \simeq +24°$. (a) White-light image taken by the Debrecen Observatory at 10:16 UT on 1977 September 5. (b) MW magnetogram recorded at 17:44 UT. (c) NSO/KP magnetogram recorded at 14:10 UT. Red line: DPD/UPP ($\gamma = 19\overset{\circ}{.}0$). Blue line: MW/MAG ($\gamma = 29\overset{\circ}{.}3$). Green line: KP/MAG ($\gamma = 39\overset{\circ}{.}5$). The magnetic measurements give larger tilt angles than DPD/UPP because the axis defined by the plage areas is steeper than that defined by the sunspots. The DPD/U measurement (not plotted) has the centroid of the following sector coinciding with a very small satellite umbra within the leading sunspot, giving a tilt angle of $12\overset{\circ}{.}3$.

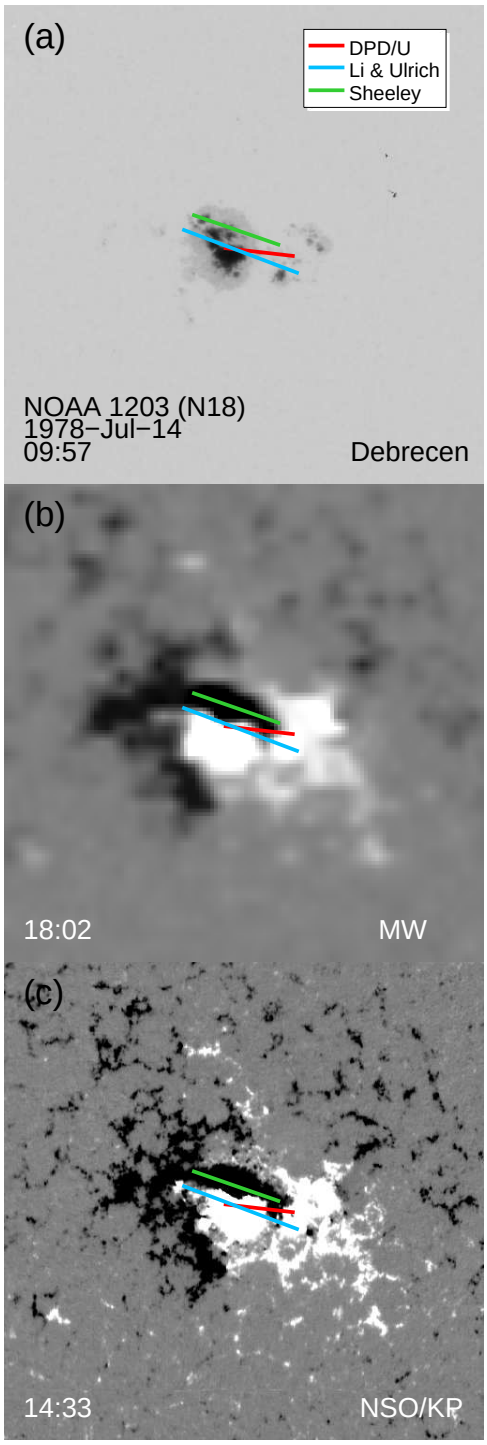

Fig. 12.— Comparison of white-light and magnetic tilt-angle measurements for NOAA 1203, centered at $L \simeq +18°$. (a) White-light image taken by the Debrecen Observatory at 09:57 UT on 1978 July 14. (b) MW magnetogram recorded at 18:02 UT. (c) NSO/KP magnetogram recorded at 14:33 UT. Red line: DPD/U ($\gamma = 6\overset{\circ}{.}4$). Blue line: MW/MAG ($\gamma = 21\overset{\circ}{.}0$). Green line: KP/MAG ($\gamma = 19\overset{\circ}{.}4$). In this case, the white-light measurements have the following sector centered on the large, eastern sunspot structure, whereas the magnetograms show that the equatorward half of this structure actually has leading polarity. The magnetic axis thus has a larger inclination than suggested by the white-light image.

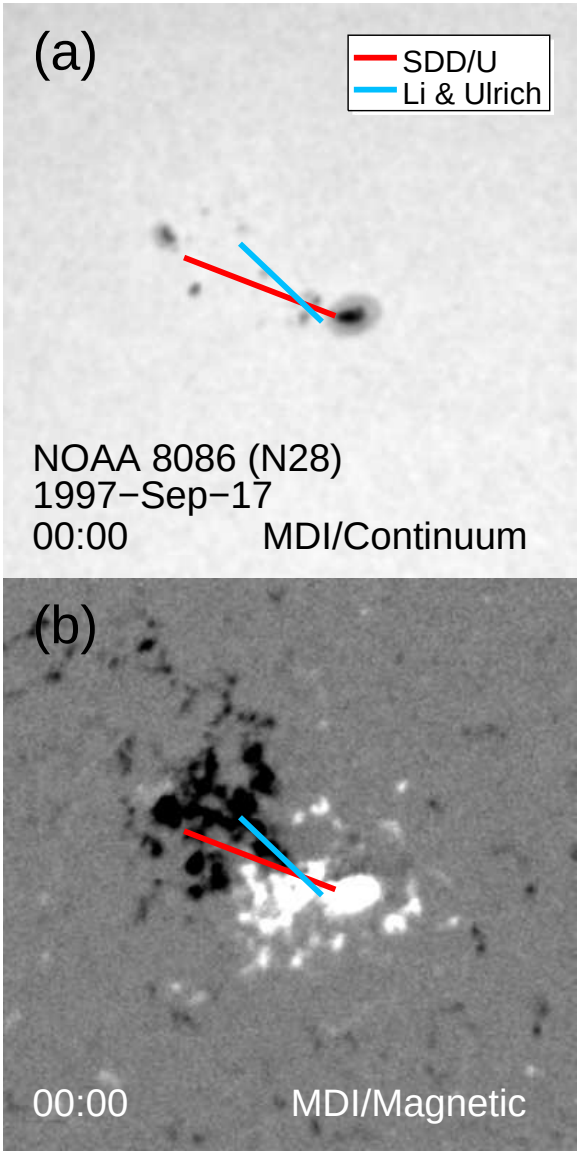

Fig. 13.— Comparison of white-light and magnetic tilt-angle measurements for NOAA 8086, centered at $L \simeq +28°$. (a) MDI continuum image recorded at 00:00 UT on 1997 September 17. (b) Simultaneous MDI magnetogram. Red line: SDD/U ($\gamma = 19\overset{\circ}{.}55$). Blue line: MDI/MAG ($\gamma = 40\overset{\circ}{.}8$; Li & Ulrich 2012). Again, the magnetic tilt angle is larger because the plage areas visible in the magnetogram have a more steeply inclined axis than the sunspots seen in the continuum image.